Christian-Albrechts-Universität zu Kiel

Lithospheric research - Petrological-geophysical modeling of the lithosphere

Jörg Ebbing

Joint Inversion Summer School
Barcelonnette, June 18th 2015

Joint inversion for the lithosphere

Christian-Albrechts-Universität zu Kiel

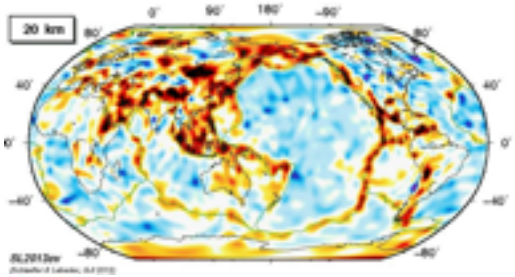

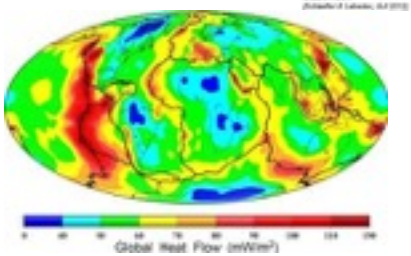

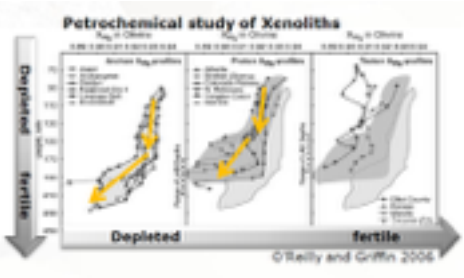

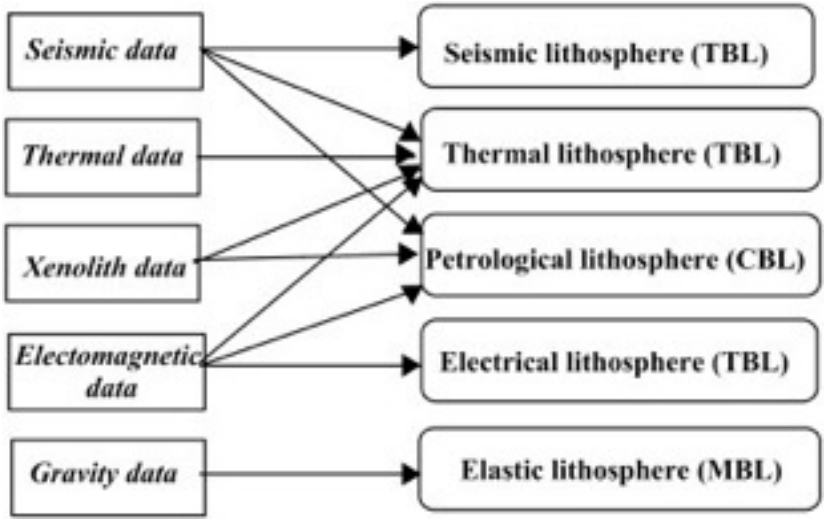

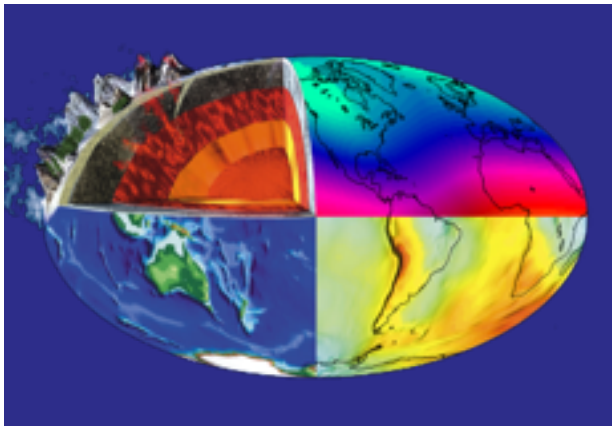

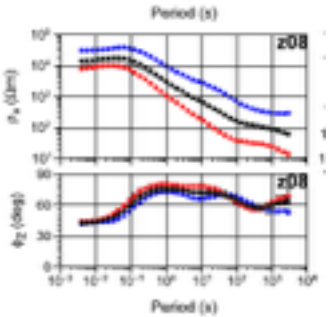

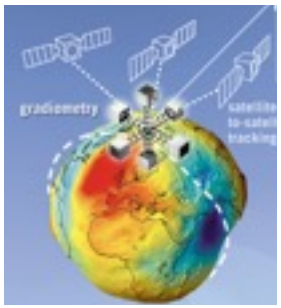

Topics

Christian-Albrechts-Universität zu Kiel

Definition of the lithosphere
- Geophysical data
- Modelling concepts

Satellite gravity and the lithosphere
- Combination with seismic tomography

Joint inversion for petrology, gravity and seimology

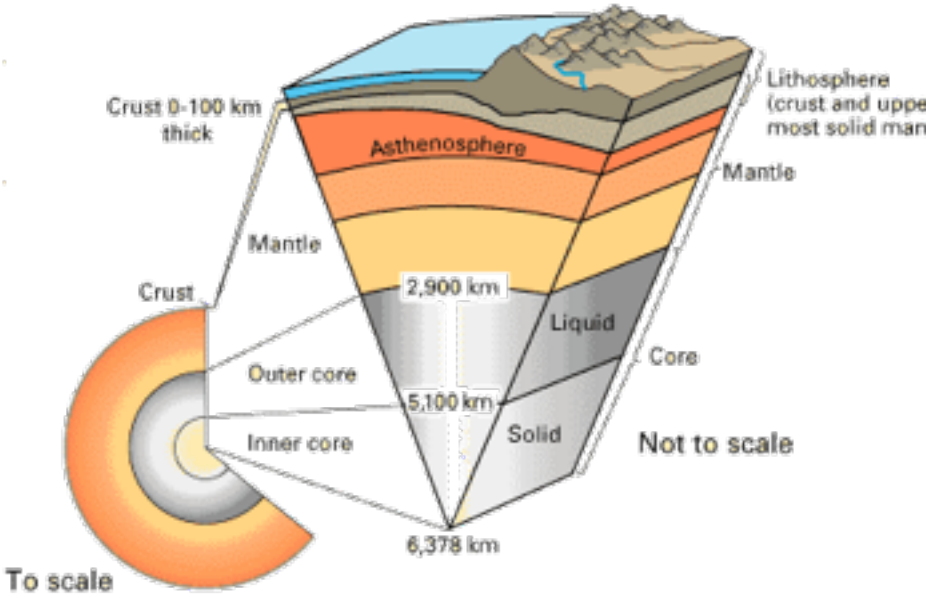

Definition of the base lithosphere

Christian-Albrechts-Universität zu Kiel

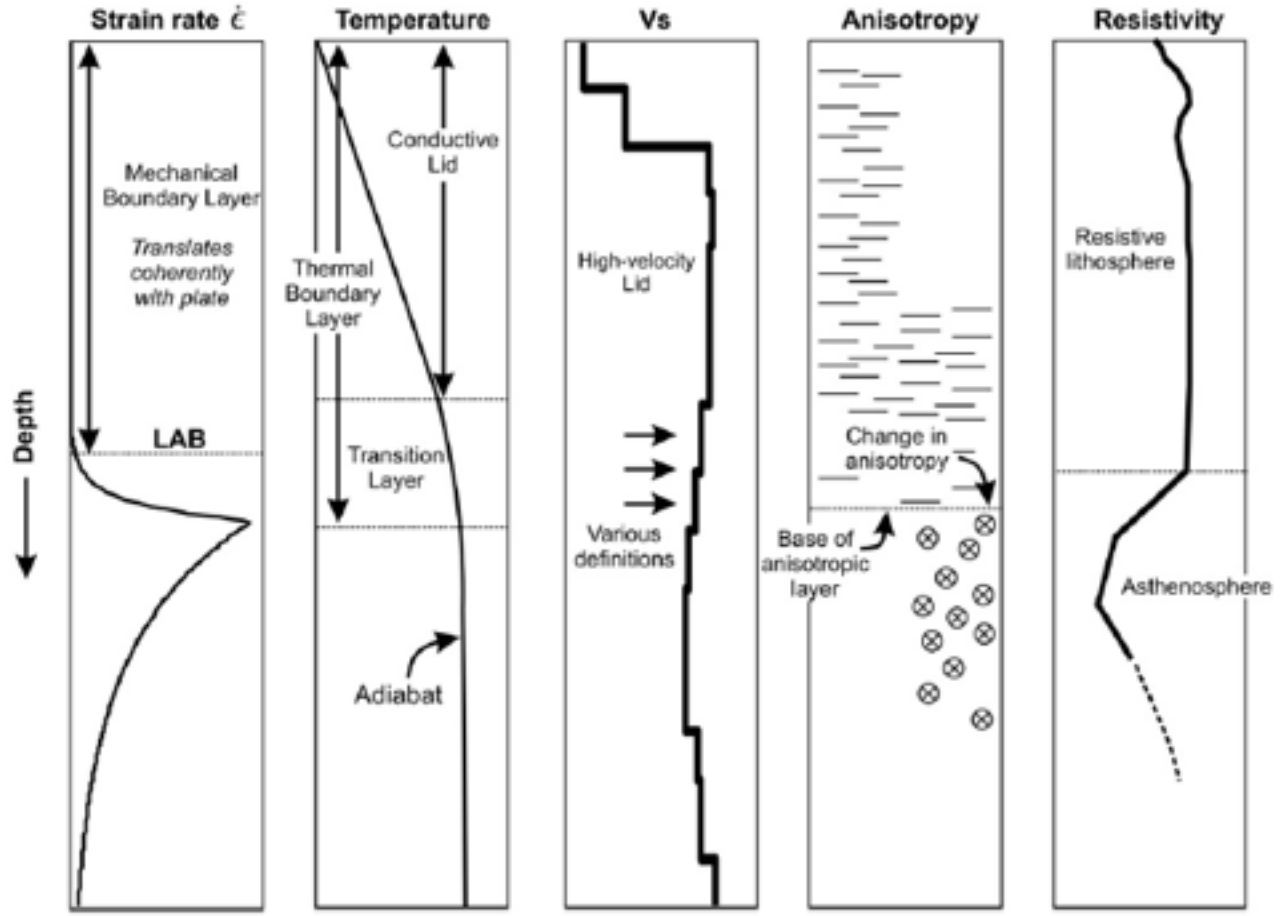

Fig. 1. Definition of the lithosphere and common proxies used to estimate its thickness. The lithosphere, *sensu stricto*, is a mechanical boundary layer (left). The lithosphere–asthenosphere boundary (LAB) coincides with the top of a zone of decoupling between the lithosphere and asthenosphere, marked by an increased strain rate. The thermal boundary layer (TBL), containing a conductive lid and a transition layer, represents a near-surface region where temperature deviates from the adiabat. A zone of low seismic shear-wave velocity (Vs) is sometimes detected beneath a high-velocity lid; various definitions have been used to correlate this zone with the LAB (see text). The LAB may also correlate with a downward extinction of seismic anisotropy (e.g., Gaherty and Jordan, 1995) or a change in the direction of anisotropy (e.g., Debayle and Kennett, 2000a; 2000b; Sebai et al., 2006). The electrical LAB is marked by a significant reduction in electrical resistivity.

Eaton et al. 2009

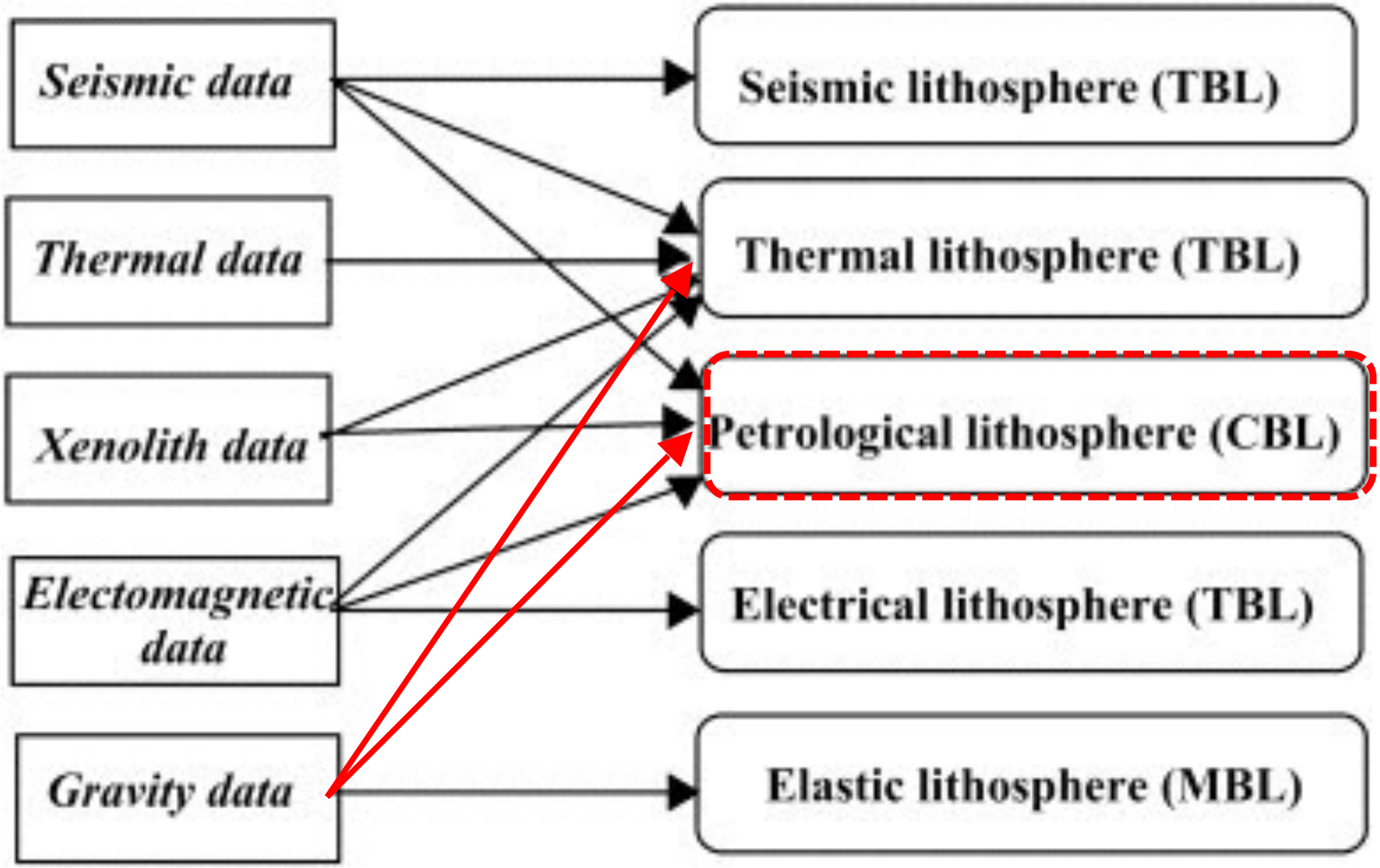

Artemieva 2009

(a) thermal lithosphere thickness

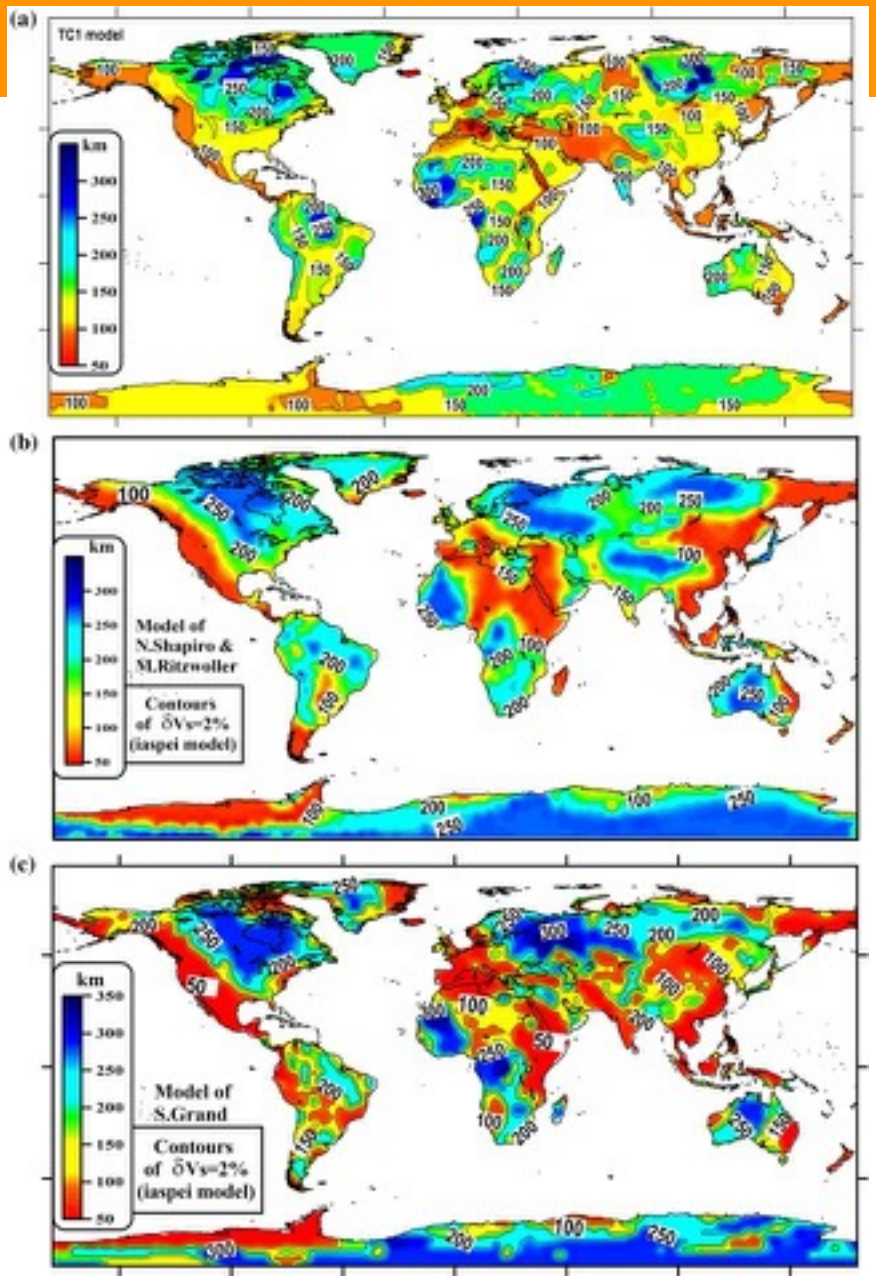

Artemieva 2009

(a) thermal lithosphere thickness

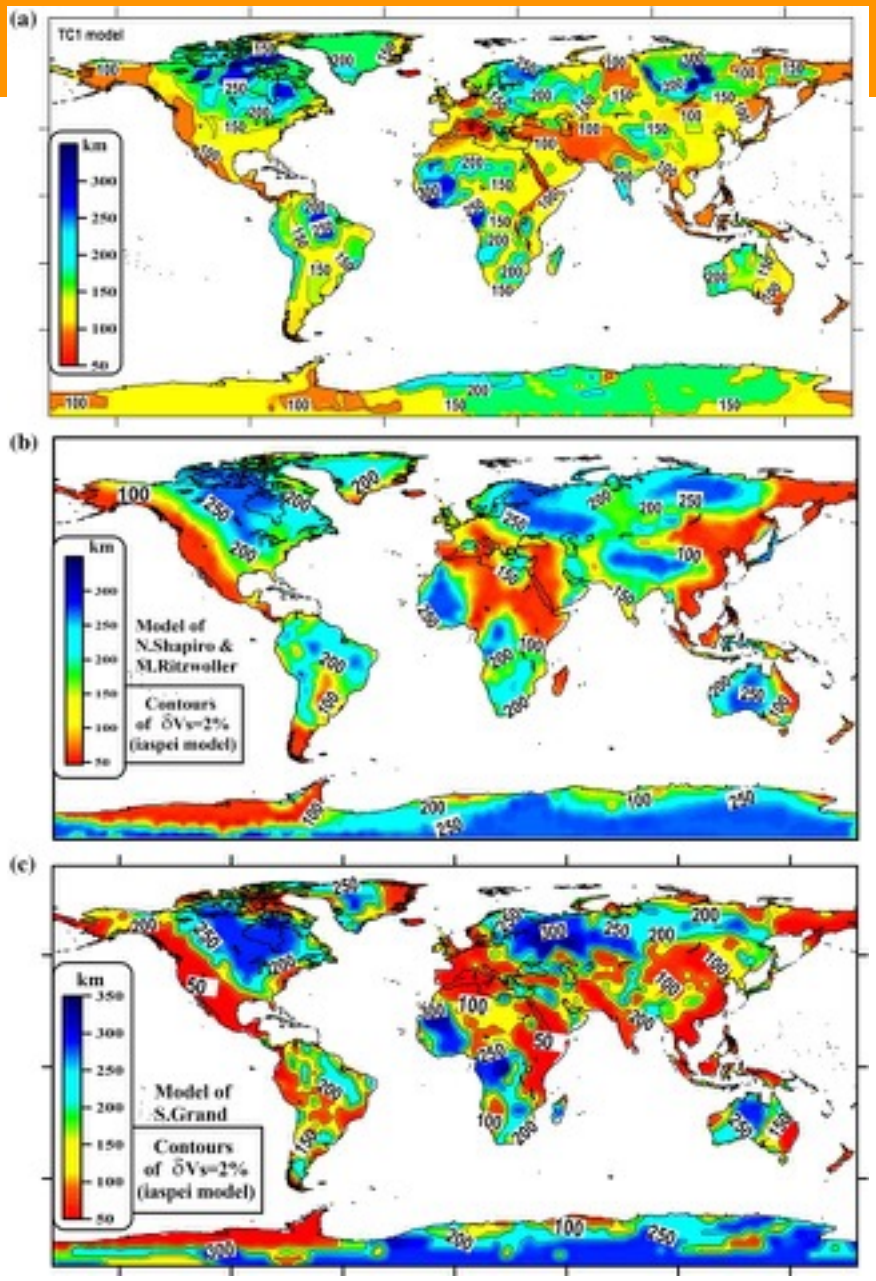

Tectonothermal age

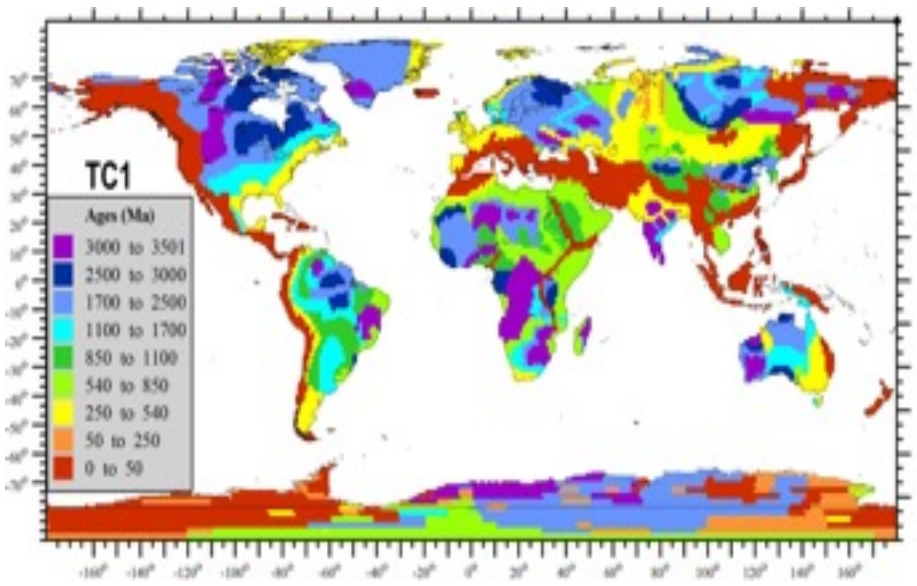

Artemieva 2009

Thickness of the continental lithosphere as defined from:
thermal modeling complemented by global statistical data on mantle temperatures

Artemieva 2009

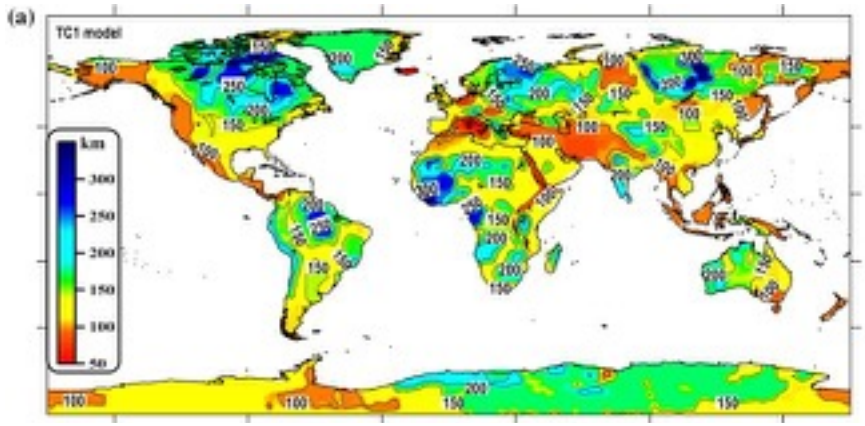

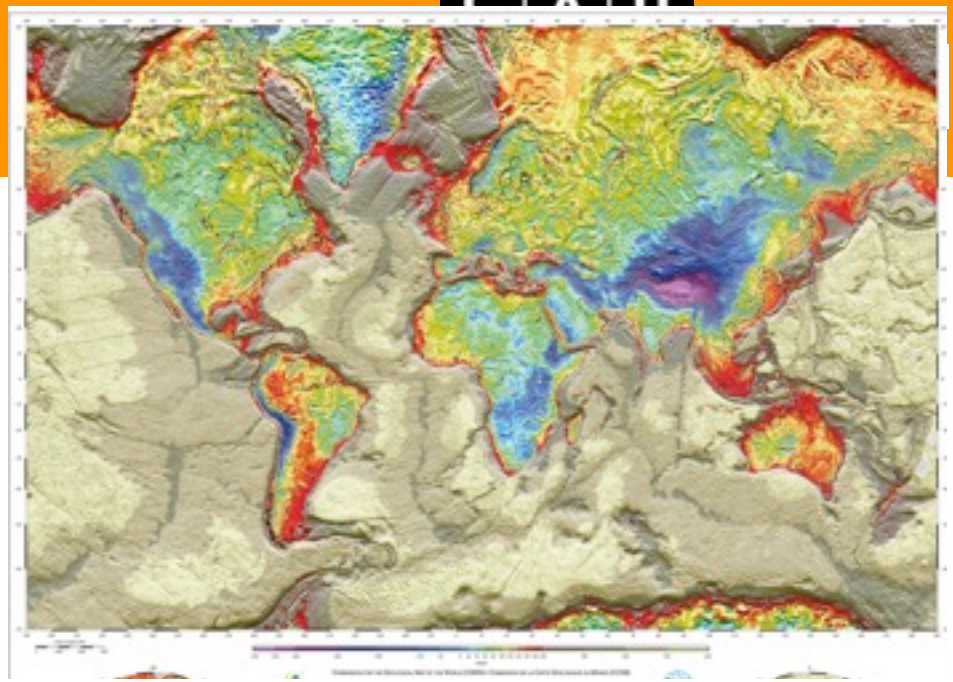

Global Bouguer anomaly

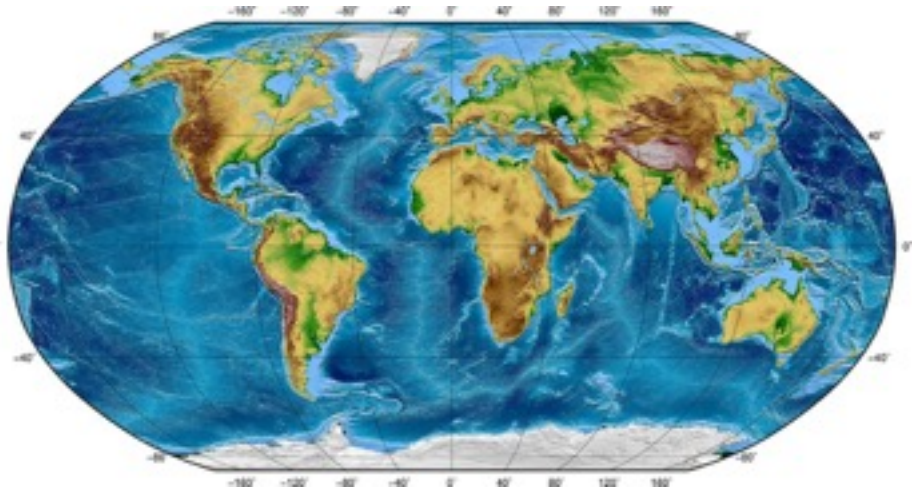

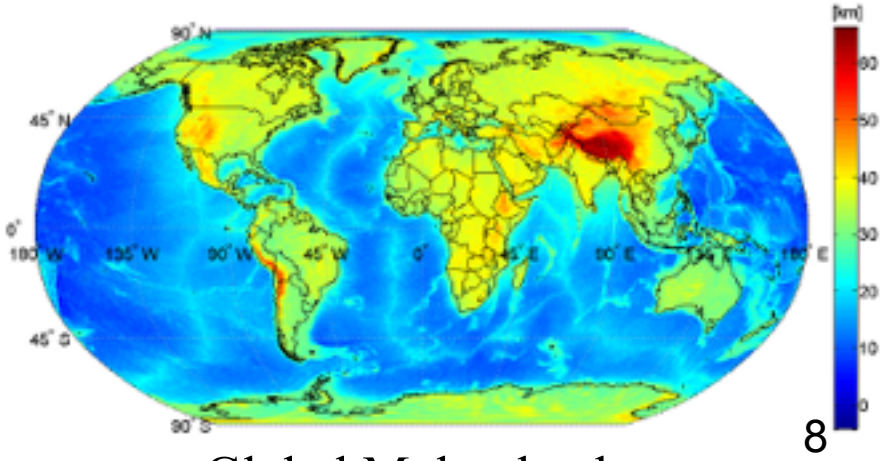

Global Moho depth

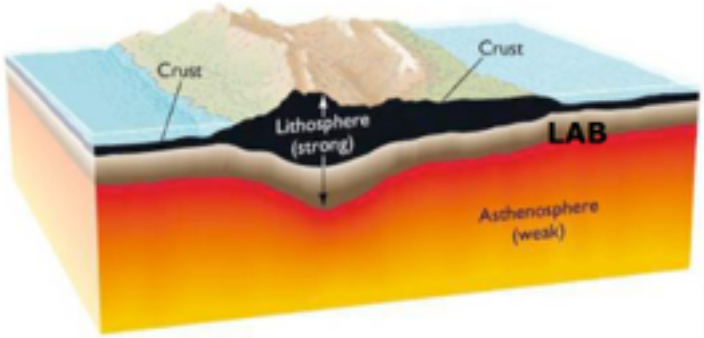

The Subcontinental Lithospheric Mantle - SCLM

Archean > 2.5 Ga | Proterozoic 2.5-1 Ga | Phanerozoic < 1 Ga

Cold — Temperature — warm

Thick — Thickness — thin

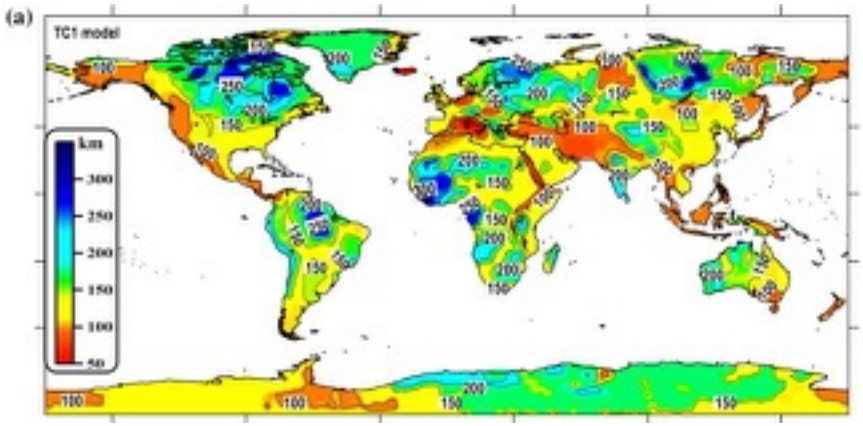

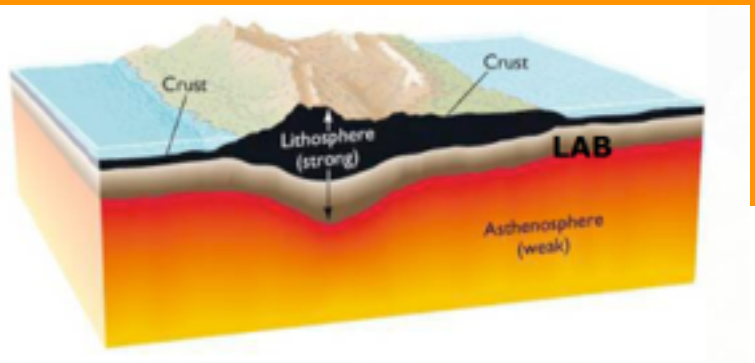

Christian-Albrechts-Universität zu Kiel

The Subcontinental Lithospheric Mantle - SCLM

Archean > 2.5 Ga

Proterozoic 2.5-1 Ga

Phanerozoic < 1 Ga

Cold — Temperature — warm

Thick — Thickness — thin

Depleted — Composition — fertile

high — Velocities — low

Density structure of lithospheric mantle

Christian-Albrechts-Universität zu Kiel

- Generally assumed that temperature is the main control on velocity – density relationship (increase temperature, decrease density)

- After Jordan (1975) craton keel is low density, but high seismic velocity due to increase in Mg#

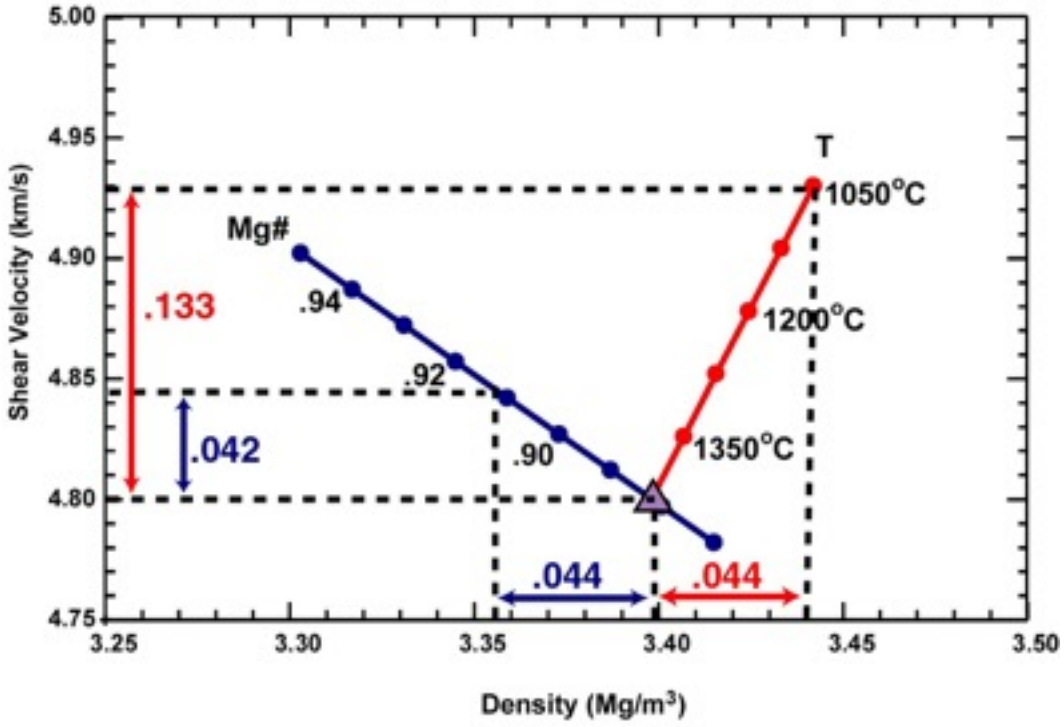

Webb 2008

Isopycnic (Equal-Density) Hypothesis

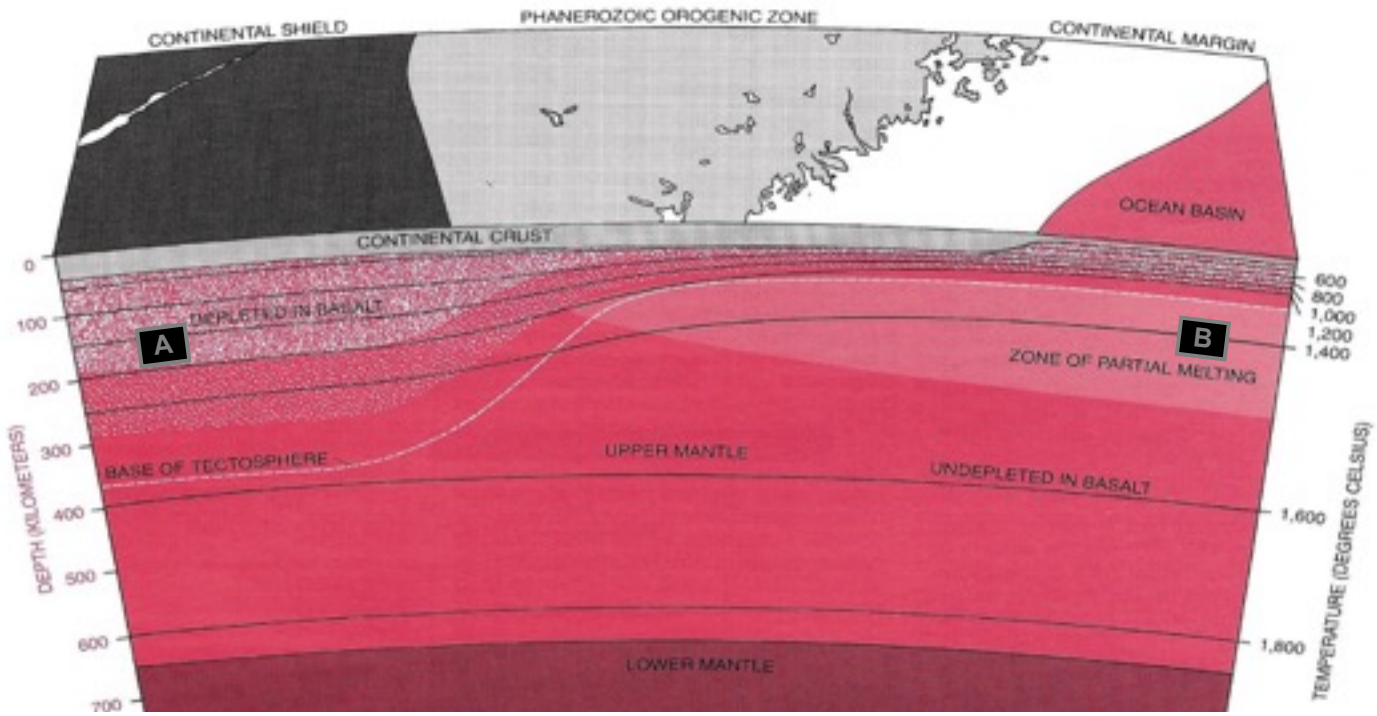

The temperature difference between the cratonic tectosphere and the convecting mantle is density-compensated by the depletion of the tectosphere in Fe and Al relative to Mg by the extraction of mafic fluids.

Courtesy of Tom Jordan

A synthetic example

Christian-Albrechts-Universität zu Kiel

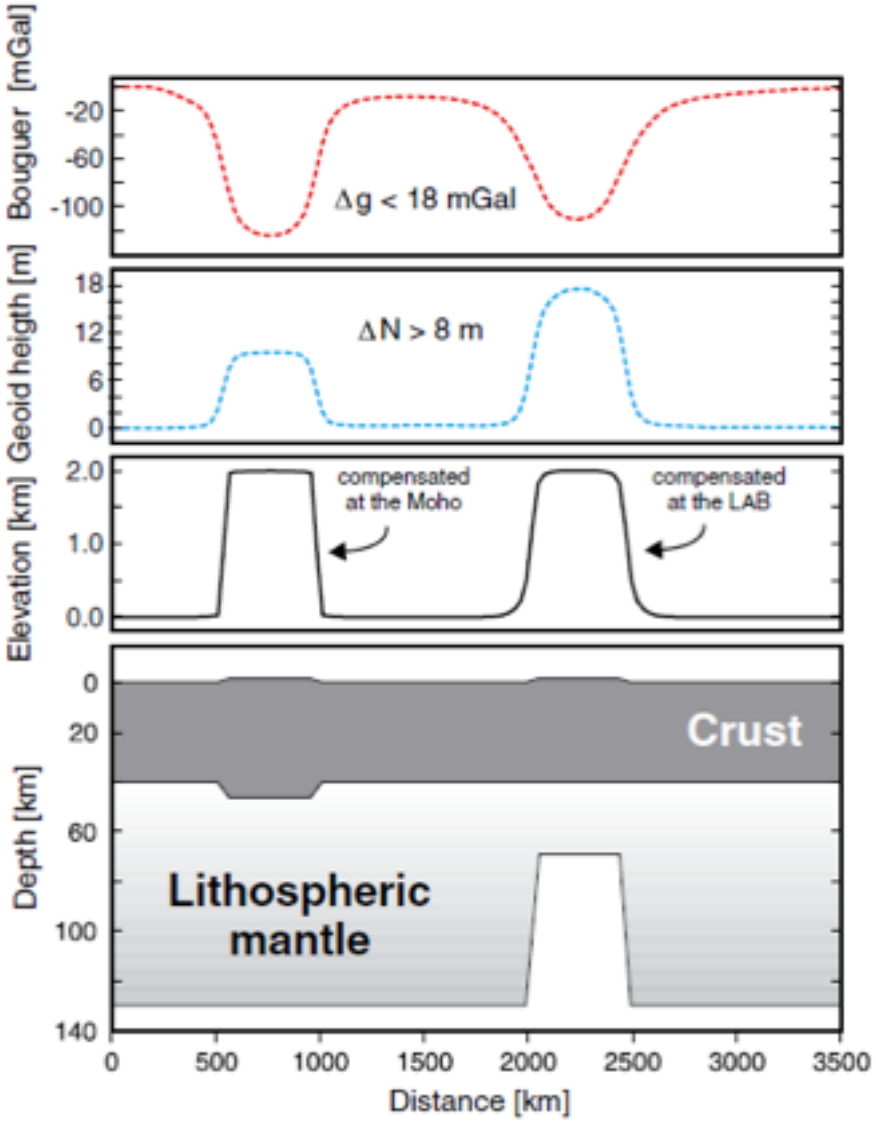

Bouguer and geoid anomalies associated with two topographic heights.
Both heights have the same absolute elevation, but their isostatic compensation is achieved at different depths. The bottom of the lithosphere (LAB) is defined as the 1315°C isotherm.

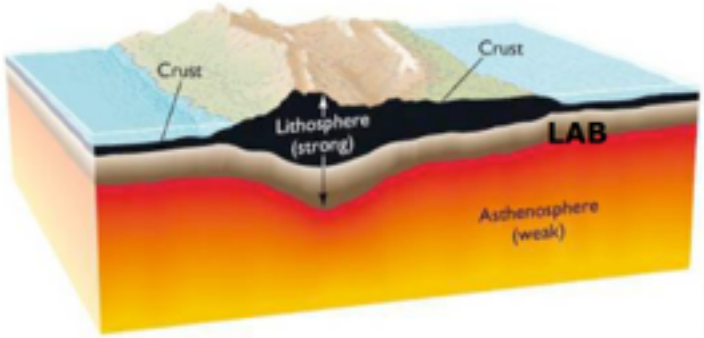

The Subcontinental Lithospheric Mantle - SCLM

Archean > 2.5 Ga | Proterozoic 2.5-1 Ga | Phanerozoic < 1 Ga

Cold	Temperature	warm
Thick	Thickness	thin
Depleted	Composition	fertile
high	Velocities	low
Low	Densities	high

Variations of shear wave velocity and electric conductivity in 150 km depth

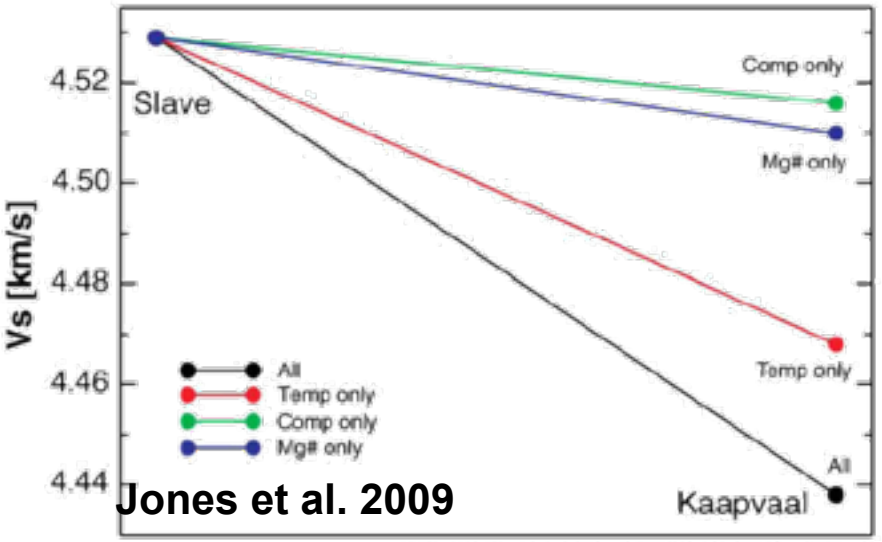

Jones et al. 2009

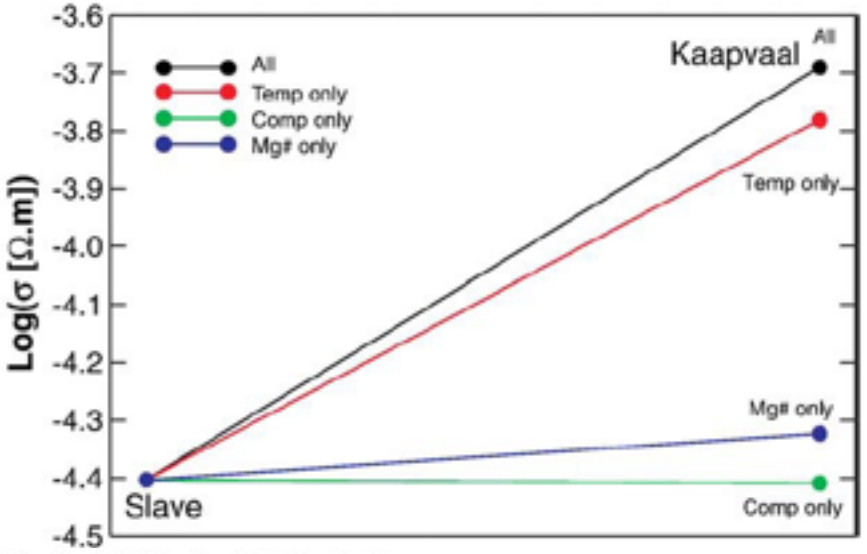

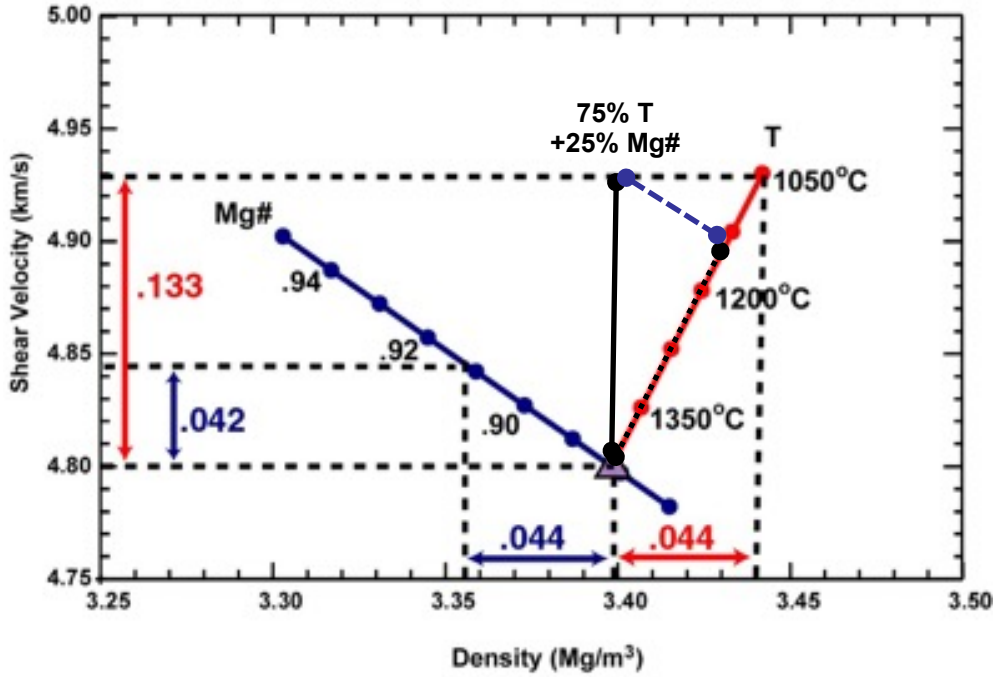

CARP Major Classes related to xenolith types

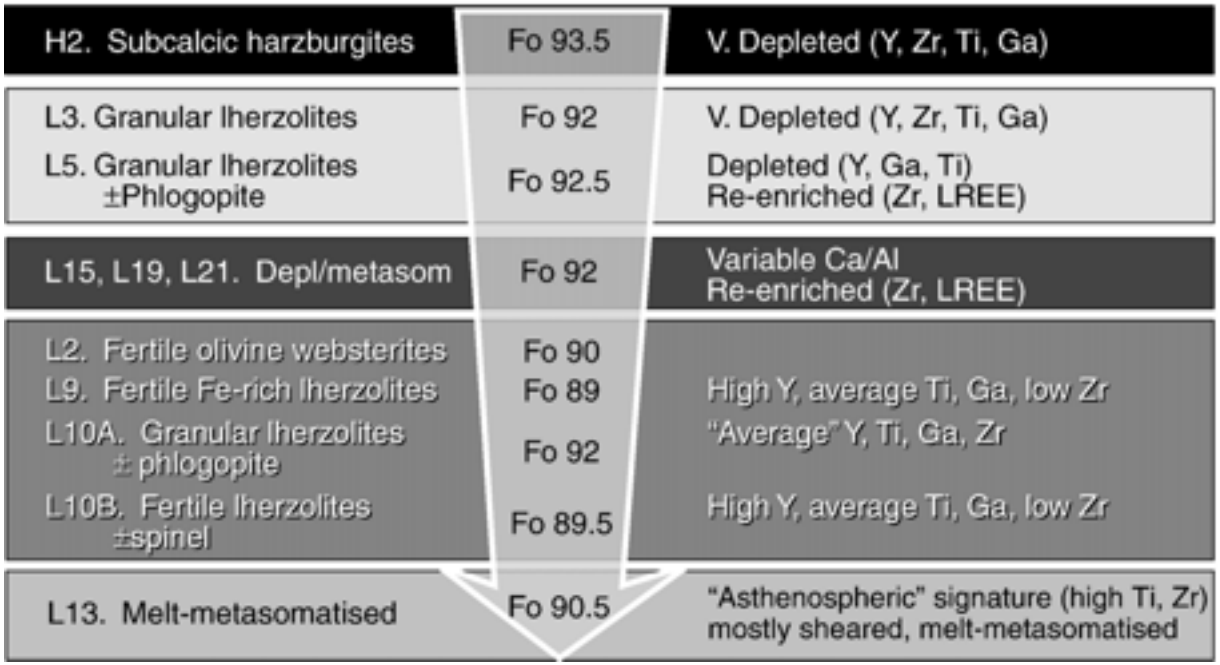

LitMod3D: Petrological-geophysical frame work

Christian-Albrechts-Universität zu Kiel

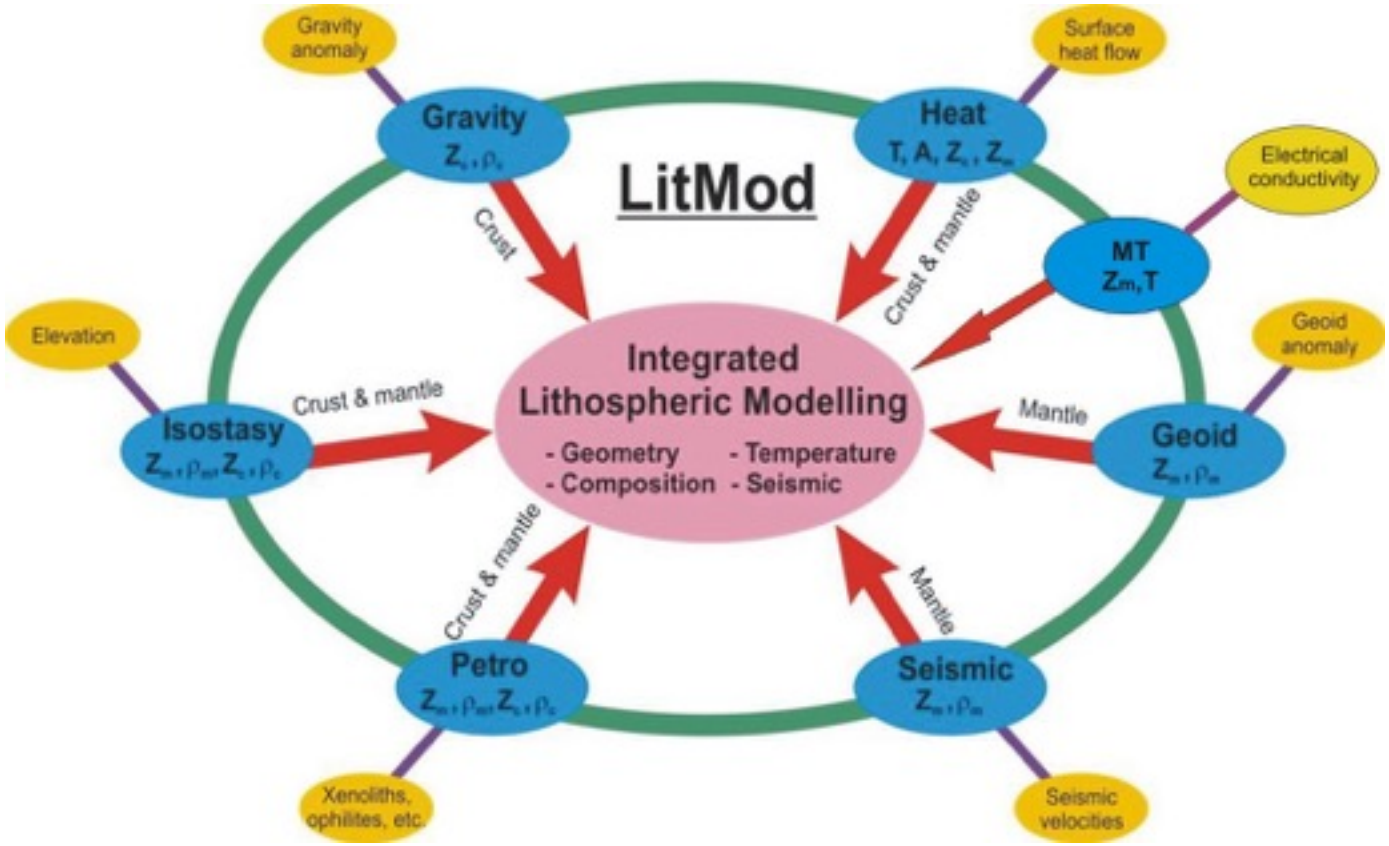

 # LitMod3D is a 3D computational code that allows to model all relevant physical properties within a robust and thermodynamically self-consistent framework.

Fullea 2011

Principle of petrological-geophysical modelling

Christian-Albrechts-Universität zu Kiel

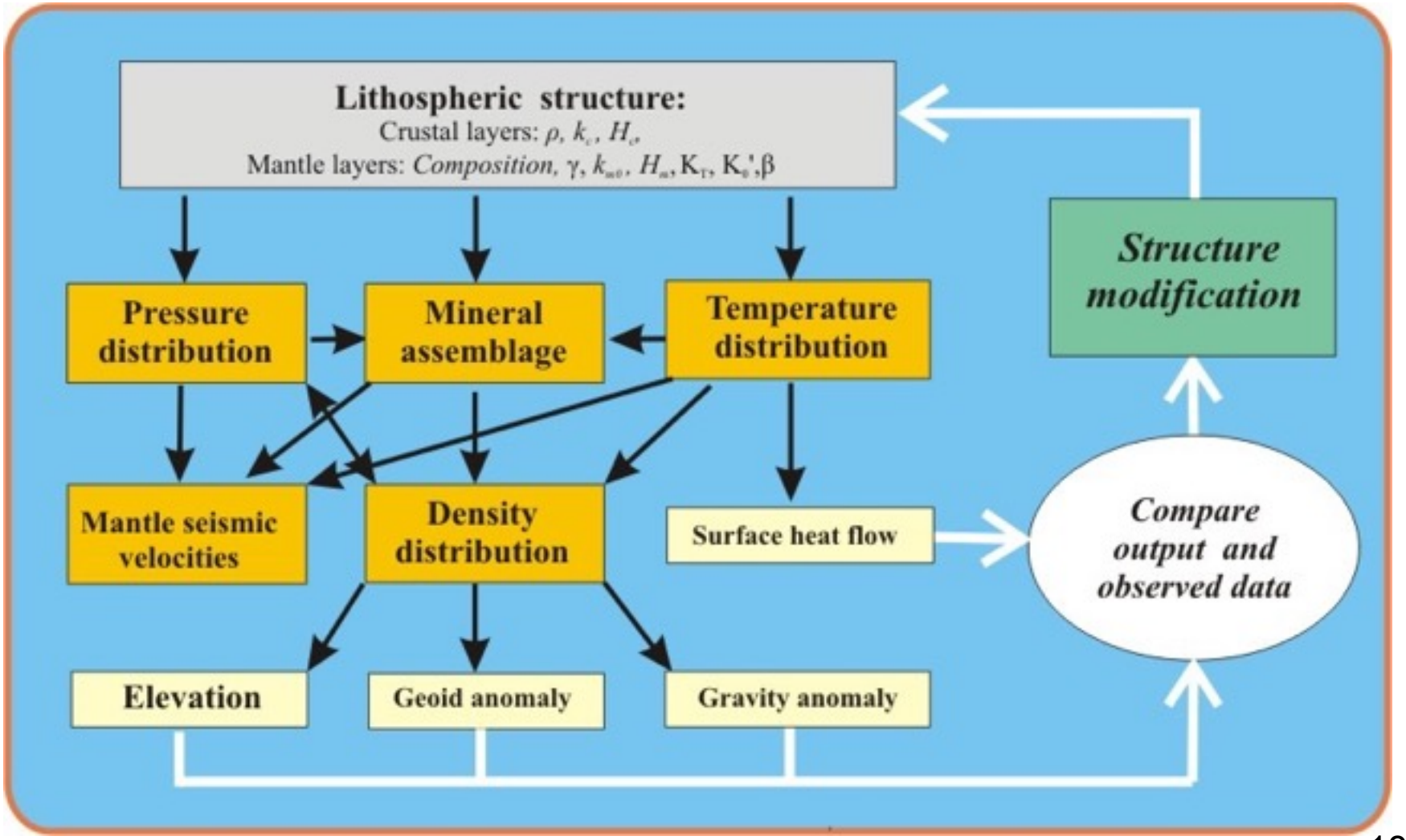

Fullea 2011

LitMod3D : Thermal field

Steady-state thermal field

Christian-Albrechts-Universität zu Kiel

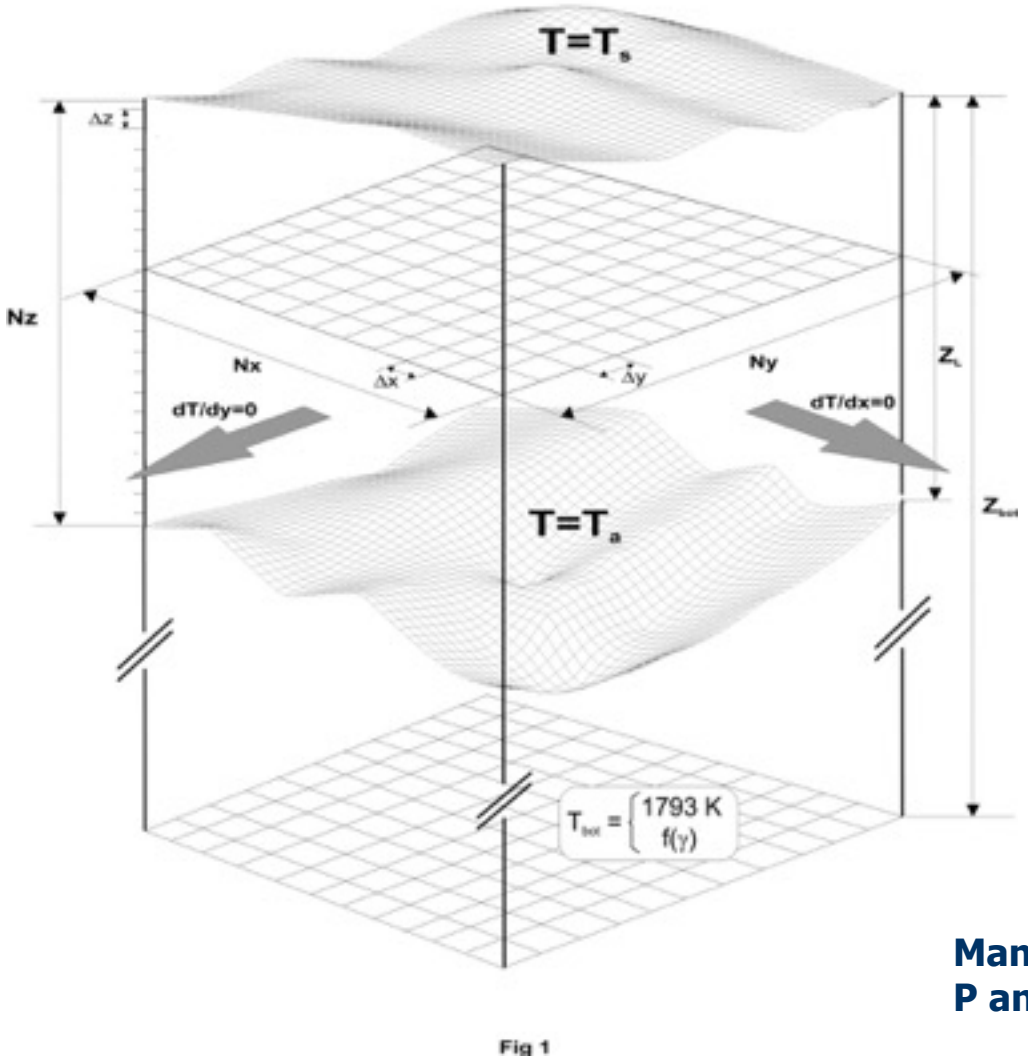

Fig 1

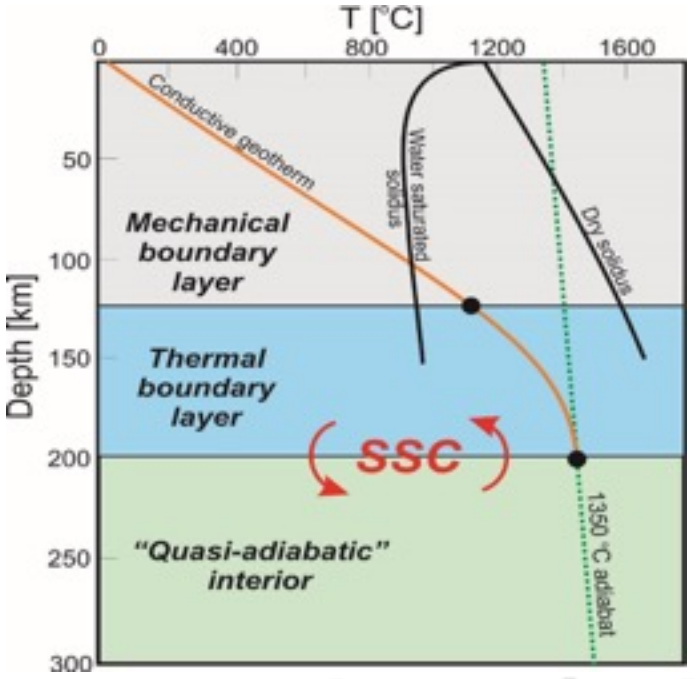

$$k_{(T,P)} = k^{\circ}\left(\frac{298}{T}\right)^{a} \exp\left[-(4\gamma + 1/3)\int_{298}^{T}\alpha(T)dt\right] \times \left(1 + \frac{K_0' P}{K_T}\right) + k_{rad}(T)$$

Mantle thermal conductivity dependent on T, P and C

LitMod3D : Thermodynamic modelling and bulk properties

Christian-Albrechts-Universität zu Kiel

All thermophysical (e.g. density and seismic velocities) properties depend ultimately on T, P, and Composition.

$$dG = V\,dP - S\,dT + \Sigma_i \mu_i\,dX_i + DdE$$

$$V = \left(\frac{\partial \mathcal{G}}{\partial P}\right)_T \qquad V\alpha = -\left(\frac{\partial \mathcal{S}}{\partial P}\right)_T = \left(\frac{\partial^2 \mathcal{G}}{\partial P \partial T}\right) \qquad C_P = -T\left(\frac{\partial^2 \mathcal{G}}{\partial T^2}\right)_P \qquad c_{ijkl} = \frac{1}{V}\left(\frac{\partial^2 \mathcal{G}}{\partial S_{ij} S_{kl}}\right)_{P,T}$$

In the mantle, stable mineral assemblages are computed by Gibbs free energy minimization either within the system CaO-FeO-MgO-Al2O3-SiO2 (CFMAS) or Na2O-CaO-FeO-MgO-Al2O3-SiO2 (NCFMAS) [*Connolly, 2005*]. Each mantle body is therefore characterized by a specific major-element composition (in wt.%), which translates into specific bulk-rock properties. All necessary files containing thermodynamic information can be generated either with the freely available software Perple_X [www.**perplex**.ethz.ch, *Connolly, 2005*] or by using a simple interface provided with LitMod3D.

Mantle composition and density profile

Christian-Albrechts-Universität zu Kiel

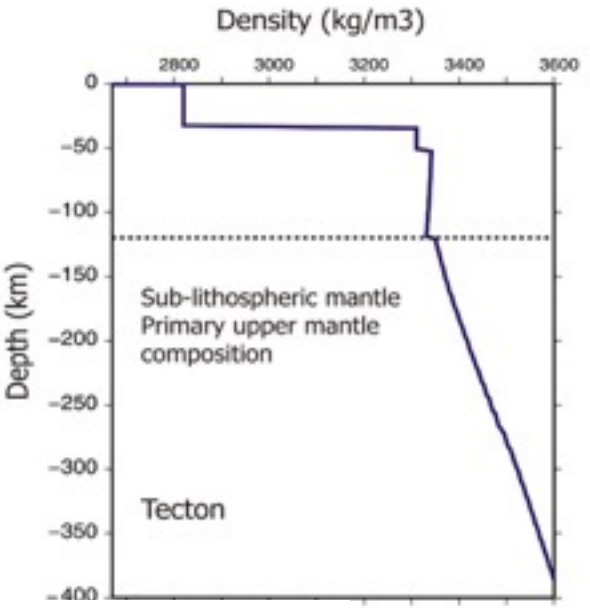

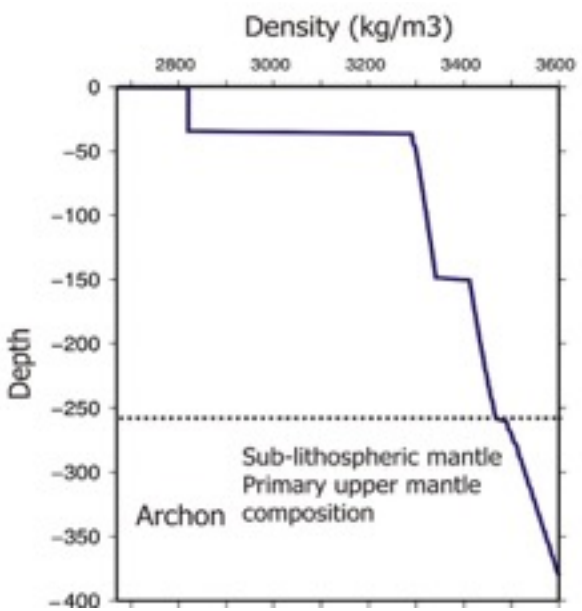

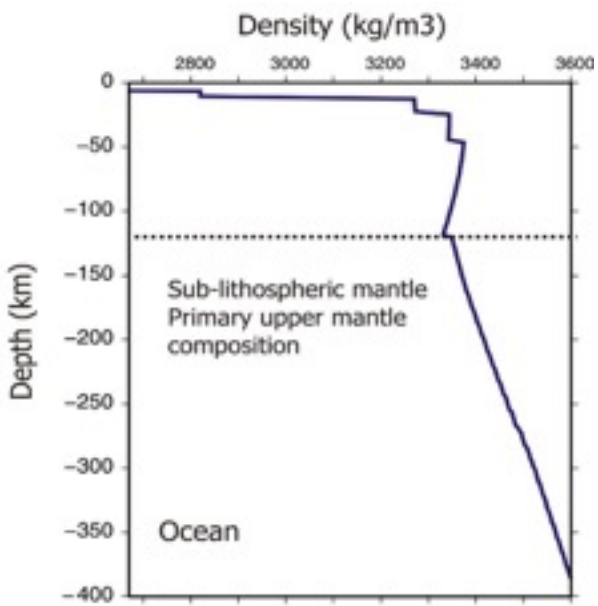

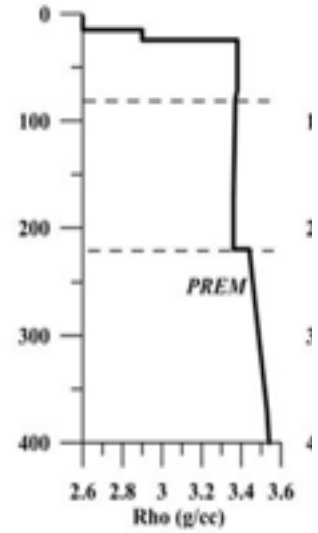

Table 1: Estimates of subcontinental lithospheric mantle compositions from xenoliths suites and peridotite massifs (modified from *Afonso et al., 2008a and Griffin et al, 2008*).

	Aver. Archon Gnt. SCLM*	Aver. Kaapvaal Harzburg.	Aver. Tecton Gnt. SCLM *	PUM J79[#]	PUM MS[#] *
SiO_2	45.7	45.9	44.5	45.2	45
TiO_2	0.04	0.05	0.14	0.22	0.2
Al_2O_3	0.99	1.3	3.5	4	4.5
Cr_2O_3	0.28	0.34	0.4	0.46	0.38
FeO	6.4	6.0	8.0	7.8	8.1
MnO	0.11	0.1	0.13	0.13	0.14
MgO	45.5	45.5	39.8	38.3	37.8
CaO	0.59	0.5	3.1	3.5	3.6
Na_2O	0.07	0.07	0.24	0.33	0.36
NiO	0.3	0.28	0.26	0.27	0.25
Mg#	92.7	93.1	89.9	89.7	89.3
Cr/(Cr+Al)	0.16	0.27	0.07	0.07	0.05

Inversion for structure and composition of the SCLM

Christian-Albrechts-Universität zu Kiel

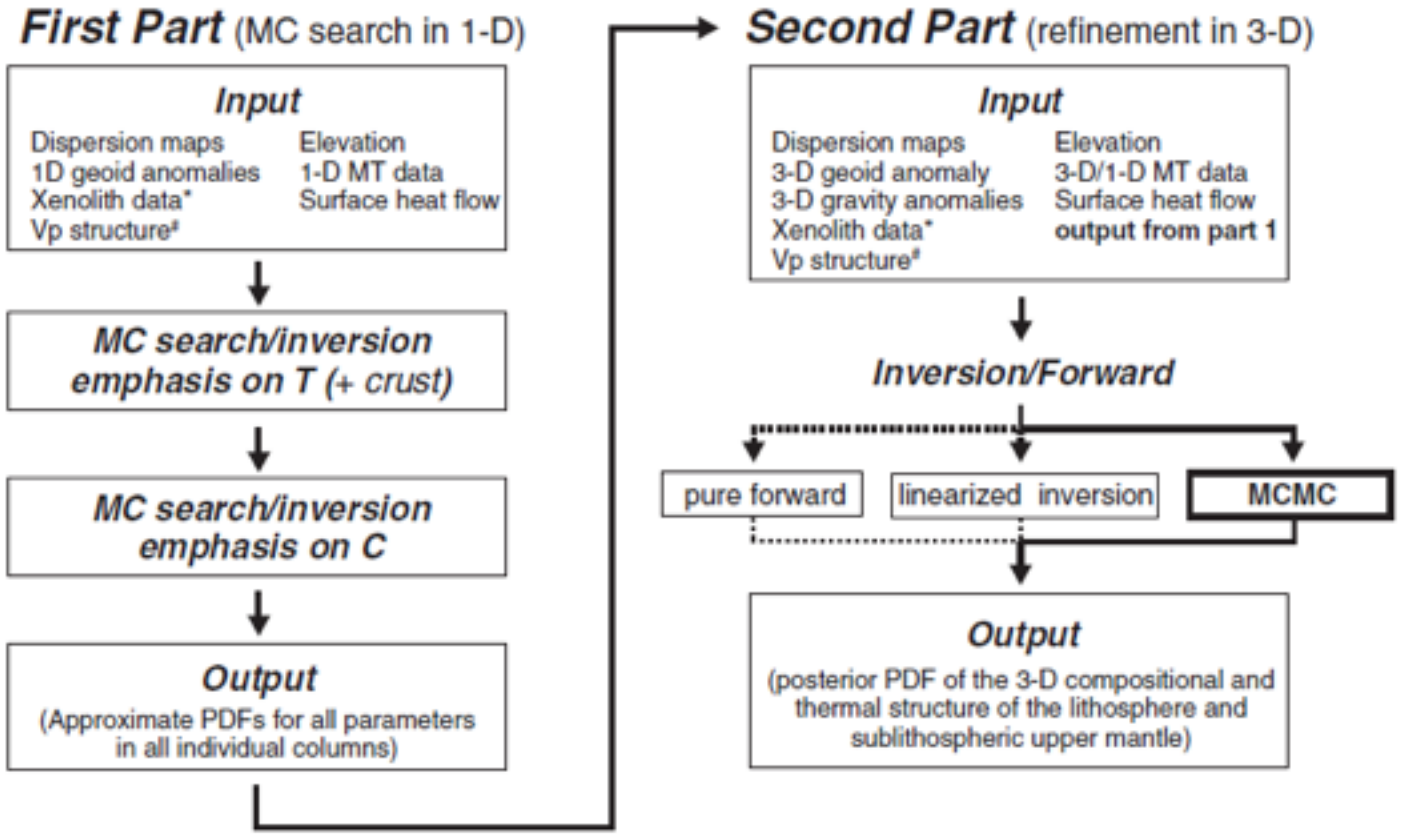

* When this information is reliable, it can be used to limit the compositional parameter space of specific compositional layers
# The present implementation uses ΔVp models only. Future implementations will include the inversion of teleseismic arrival time residuals (see text).

Multi-observable probabilistic inversions based on thermodynamic grounds offers a robust means to invert for the thermochemical structure of the Earth's mantle

Afonso et al. 2013

The *a priori* assumption: Compositional Parameters & Physical theories

Christian-Albrechts-Universität zu Kiel

- The Crust: Independent Information
- The Lithospheric Mantle: Melt Depletion and Refertilization
- Correlations Among Major Oxides
- Gibbs Energy Minimization
- Electrical Conductivity of Polymineralic Samples
- Isostasy and Elevation

$$\theta(\mathbf{d} \mid \mathbf{m}) = \propto \exp\left\{-\frac{1}{2}(\mathbf{d} - \mathbf{g}(\mathbf{m}))^T C_t^{-1}(\mathbf{d} - \mathbf{g}(\mathbf{m}))\right\}$$

Probability Density Function

Christian-Albrechts-Universität zu Kiel

Within the context of statistical inference, the most general solution to the inverse problem is represented by a joint probability density function (PDF) in the parameter and data space, σ (**d**,**m**), known as the a posteriori PDF [cf. *Mosegaard and Tarantola*, 2002; *Tarantola*, 2005; *Congdon*, 2006].

$$\sigma(\mathbf{m}) \propto \rho(\mathbf{m})\, L(\mathbf{m})$$

with

$$L(\mathbf{m}) \propto \int \rho(\mathbf{d})\, \theta(\mathbf{d} \mid \mathbf{m})\, d\mathbf{d}$$

Where ρ (**m**) is the a priori PDF describing all the information in the parameter space that is independent from the actual measurements, *L*(**m**) is the so-called *likelihood function*, which describes the probability of obtaining the observed data **d** given **m** (i.e., a measure of how good the model **m** is in explaining the data), ρ (**d**) the a priori PDF describing data uncertainties, and θ (**d** | **m**) the conditional probability describing the uncertainties associated with predictions from our theoretical models.

Inversion and discretization scales

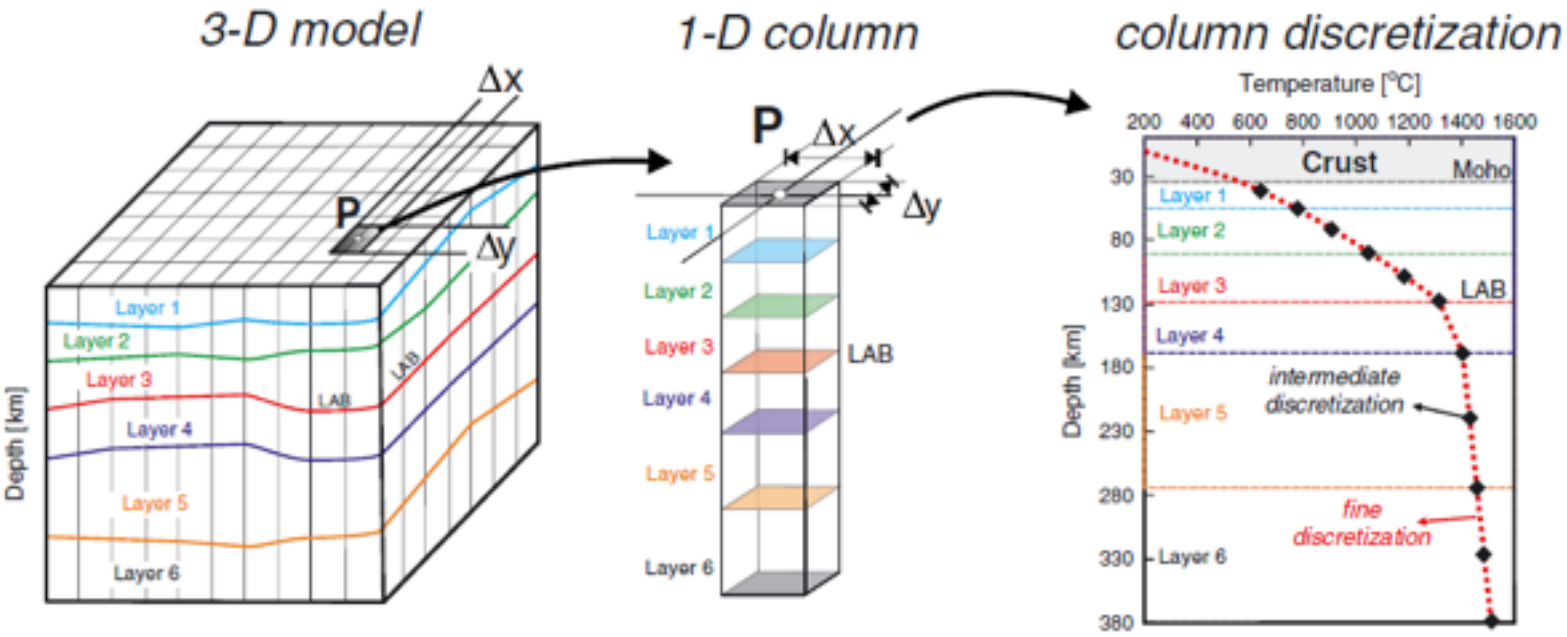

A 3-D model can be thought of as made up of a collection of 1-D columns. Each column has three discretization scales. The finest discretization scale (*computation nodes*) is used in the numerical solution of the forward problem, both in 1-D and 3-D. The intermediate discretization scale (*thermodynamic nodes*) is used in the solution of the Gibbs free energy minimization problem. Typically, 10–20 nodes are used in the intermediate discretization. The third discretization scale (*compositional layers*) refers to the actual number of independent compositional layers allowed in the model.

Afonso et al. 2013

1-D and 3-D stage inversion

Christian-Albrechts-Universität zu Kiel

The division of the inversion scheme into a preliminary 1-D stage and a final 3-D stage is sensible for the following reasons:

1. The observables used in the first 1-D stage (dispersion maps, elevation, MT data, 1-D geoid anomaly, surface heat flow) are largely controlled by the 1-D structure of the lithosphere and upper mantle.

$$N = -\frac{2\pi G}{g} \int_{\mathrm{LC}} z \cdot \rho(z) \mathrm{d}z + N_0$$

A rapid method to map the crustal and lithospheric thickness using elevation, geoid anomaly and thermal analysis

Christian-Albrechts-Universität zu Kiel

$$\int_{LC} \Delta\rho(z)\mathrm{d}z = 0$$

If local isostasy holds and the wavelength of lateral density variations is large with respect to their depth, the geoid anomaly, N, is proportional to the dipolar moment of the vertical anomalous density distribution beneath the observation point for a flat-earth model:

$$N = -\frac{2\pi G}{g}\int_{LC} z\cdot\rho(z)\mathrm{d}z + N_0$$

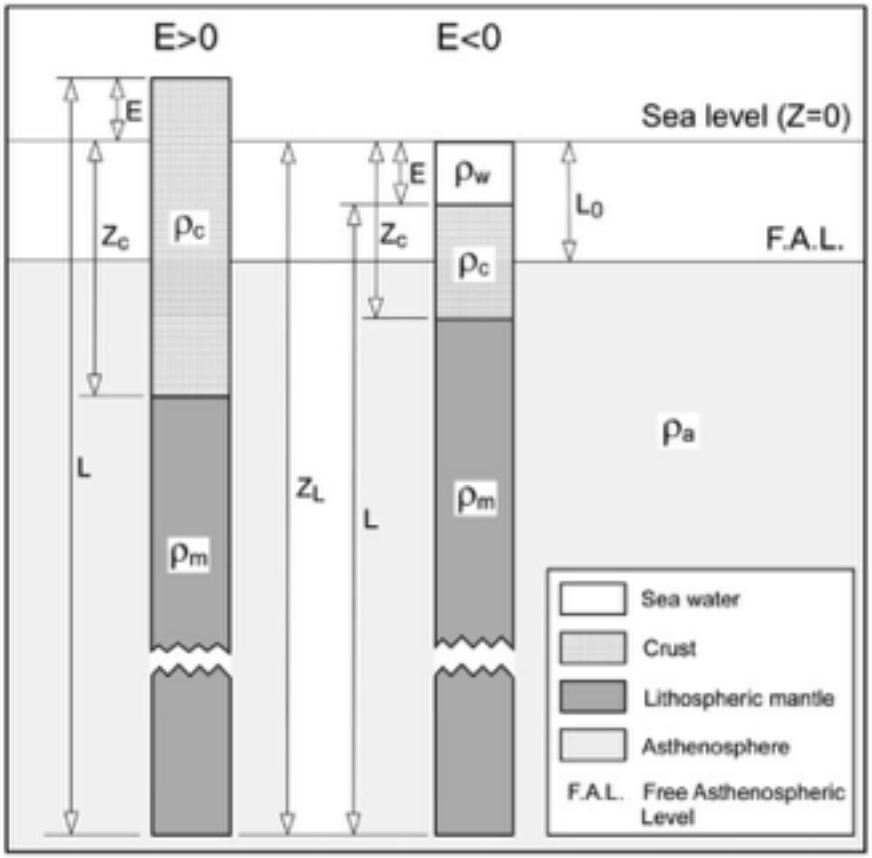

1-D and 3-D stage inversion

Christian-Albrechts-Universität zu Kiel

The division of the inversion scheme into a preliminary 1-D stage and a final 3-D stage is sensible for the following reasons:

1. The observables used in the first 1-D stage (dispersion maps, elevation, MT data, 1-D geoid anomaly, surface heat flow) are largely controlled by the 1-D structure of the lithosphere and upper mantle.

2. The initial 3-D models constructed by assembling the best-fitting 1-D columns, and used as starting models in the 3-D refinement stage, typically represent already acceptable models (i.e., they explain most of the data well).

1D synthetic example

Christian-Albrechts-Universität zu Kiel

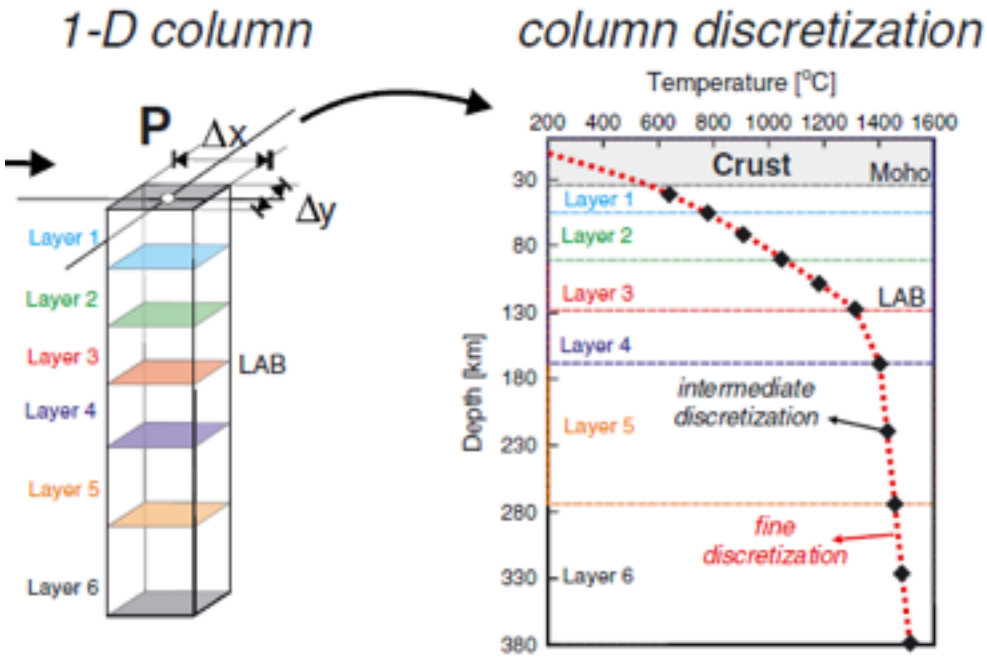

Layer #	SiO_2	Al_2O_3	FeO	MgO	CaO	Mg#
1	46.08	1.00	6.45	45.88	0.59	92.7
2	46.34	0.98	6.75	45.34	0.59	92.3
3	44.88	1.76	8.21	43.87	1.29	90.5
4	45.84	2.06	8.24	42.55	1.31	90.2
5	45.45	4.55	8.18	38.18	3.64	89.3
6	45.45	4.55	8.18	38.18	3.64	89.3

Afonso et al. 2013

Ensemble of acceptable results from 1-D column by column inversion

Christian-Albrechts-Universität zu Kiel

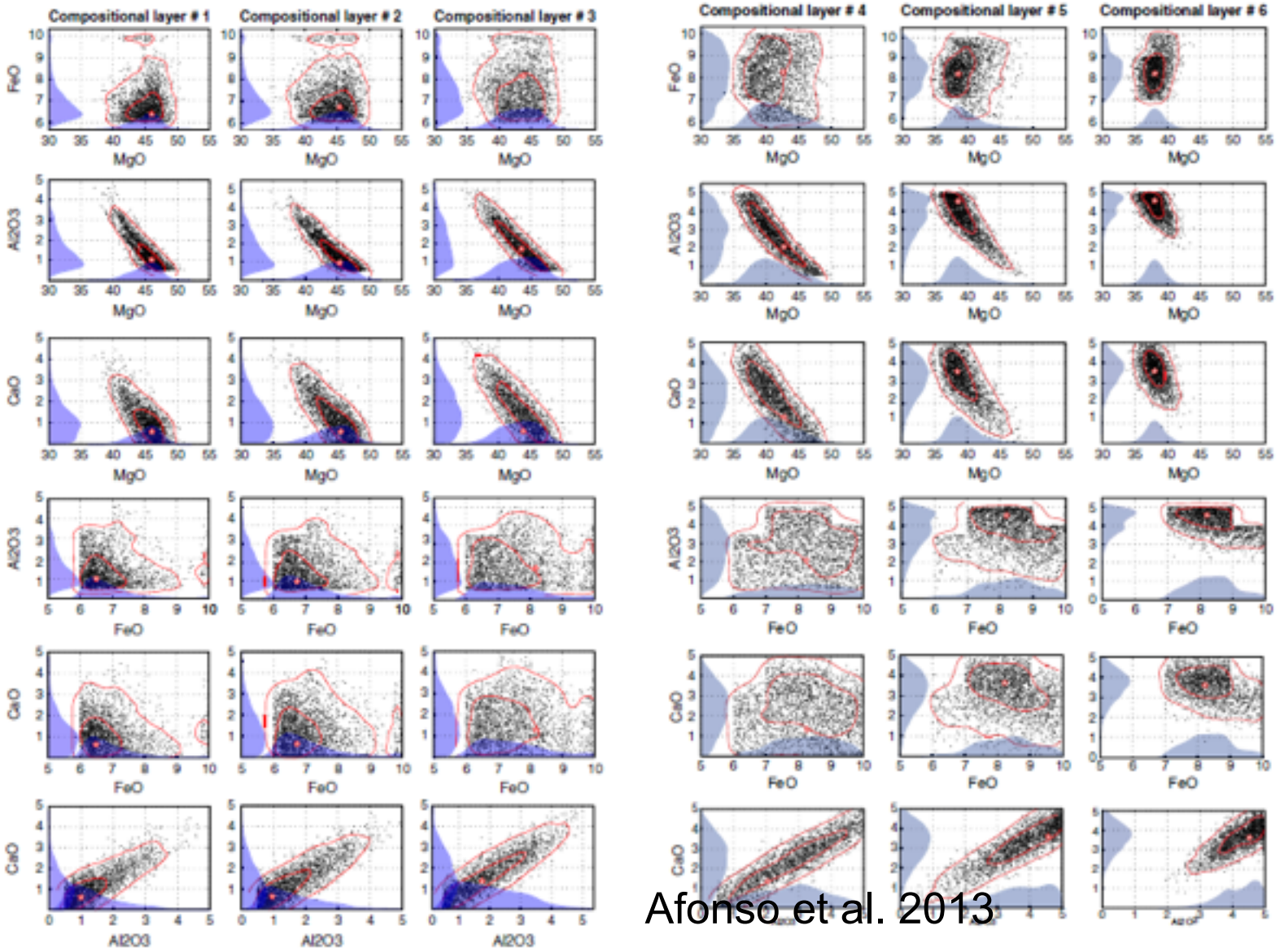

Afonso et al. 2013

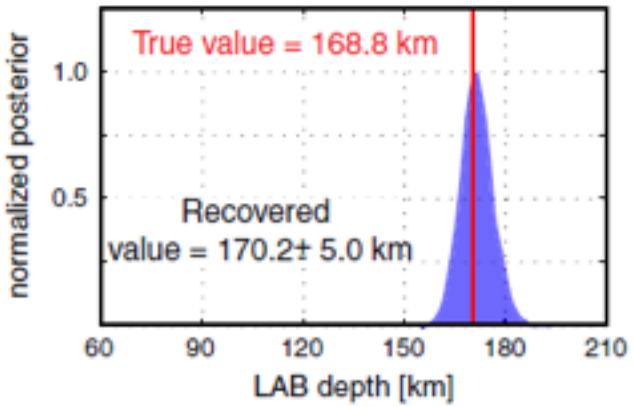

Posterior distribution obtained during the 1-D inversion/search for the LAB depth.

Layer #	SiO_2	Al_2O_3	FeO	MgO	CaO	Mg#	Mg_R#[a]
1	46.08	1.00	6.45	45.88	0.59	92.7	92 ± 0.9
2	46.34	0.98	6.75	45.34	0.59	92.3	91.7 ± 1.1
3	44.88	1.76	8.21	43.87	1.29	90.5	91.1 ± 1.2
4	45.84	2.06	8.24	42.55	1.31	90.2	90.0 ± 1.4
5	45.45	4.55	8.18	38.18	3.64	89.3	89.4 ± 1.1
6	45.45	4.55	8.18	38.18	3.64	89.3	89.0 ± 0.8

[a] Mean ± standard deviation of the recovered values.

Bulk compositions used in the synthetic model. The original and recovered Mg# of each layer is also included.

Afonso et al. 2013

3-D example: Synthetic model set-up

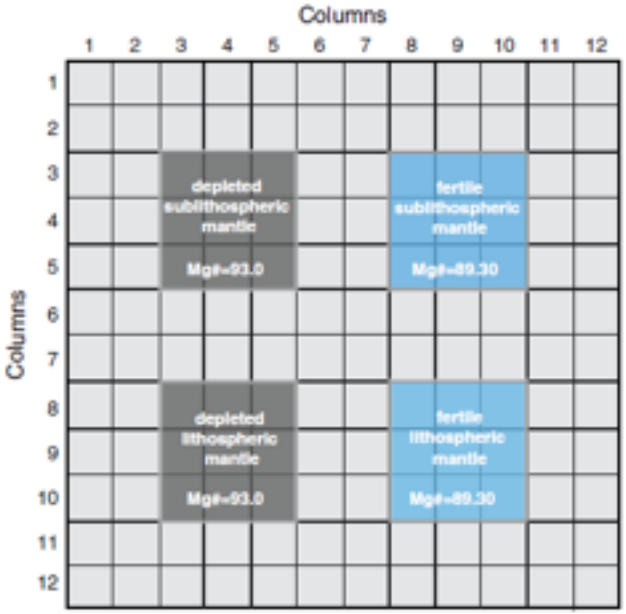

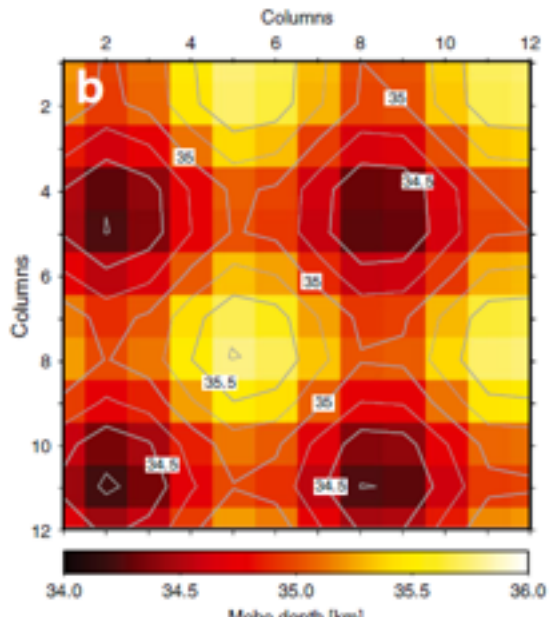

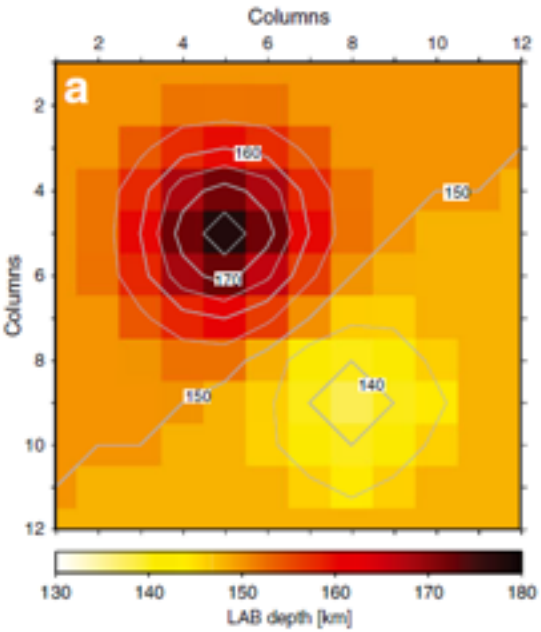

Afonso et al. 2013

Geophysical «observables»

Christian-Albrechts-Universität zu Kiel

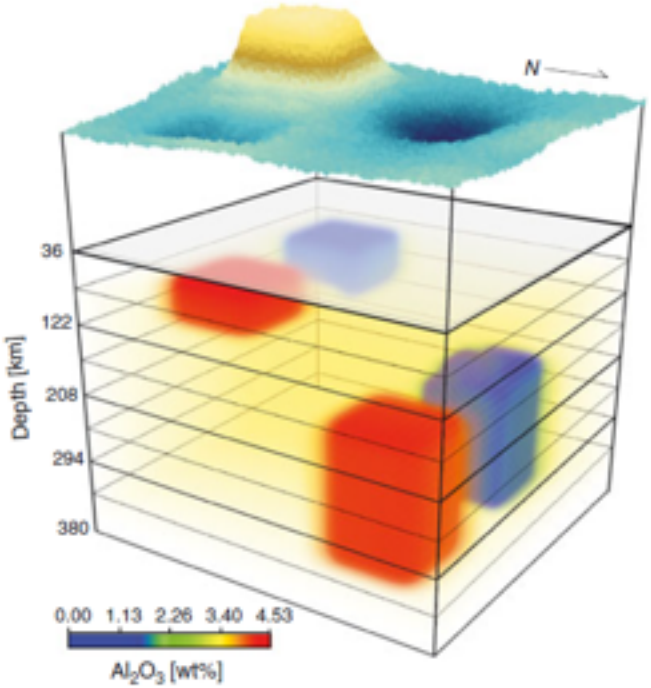

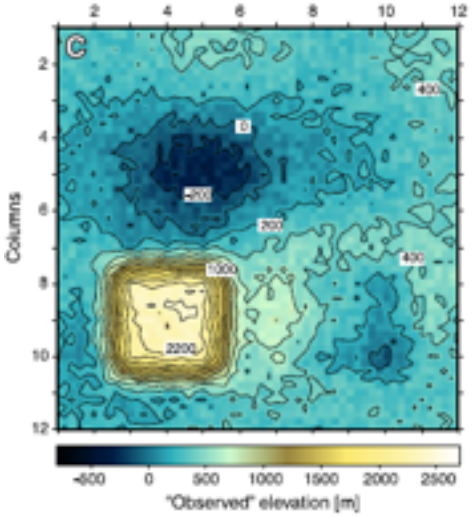

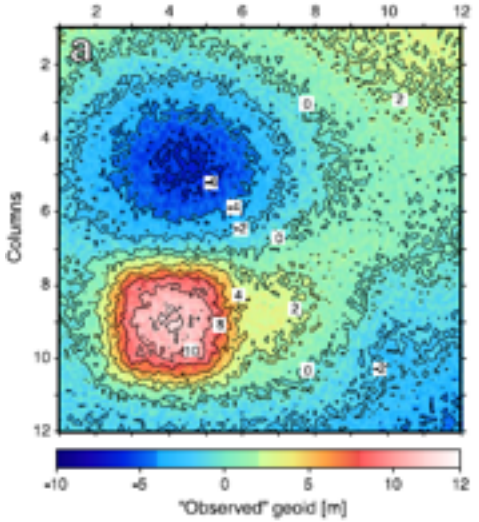

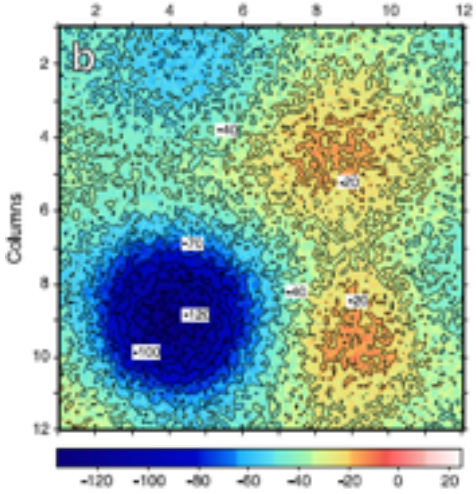

Inverse results

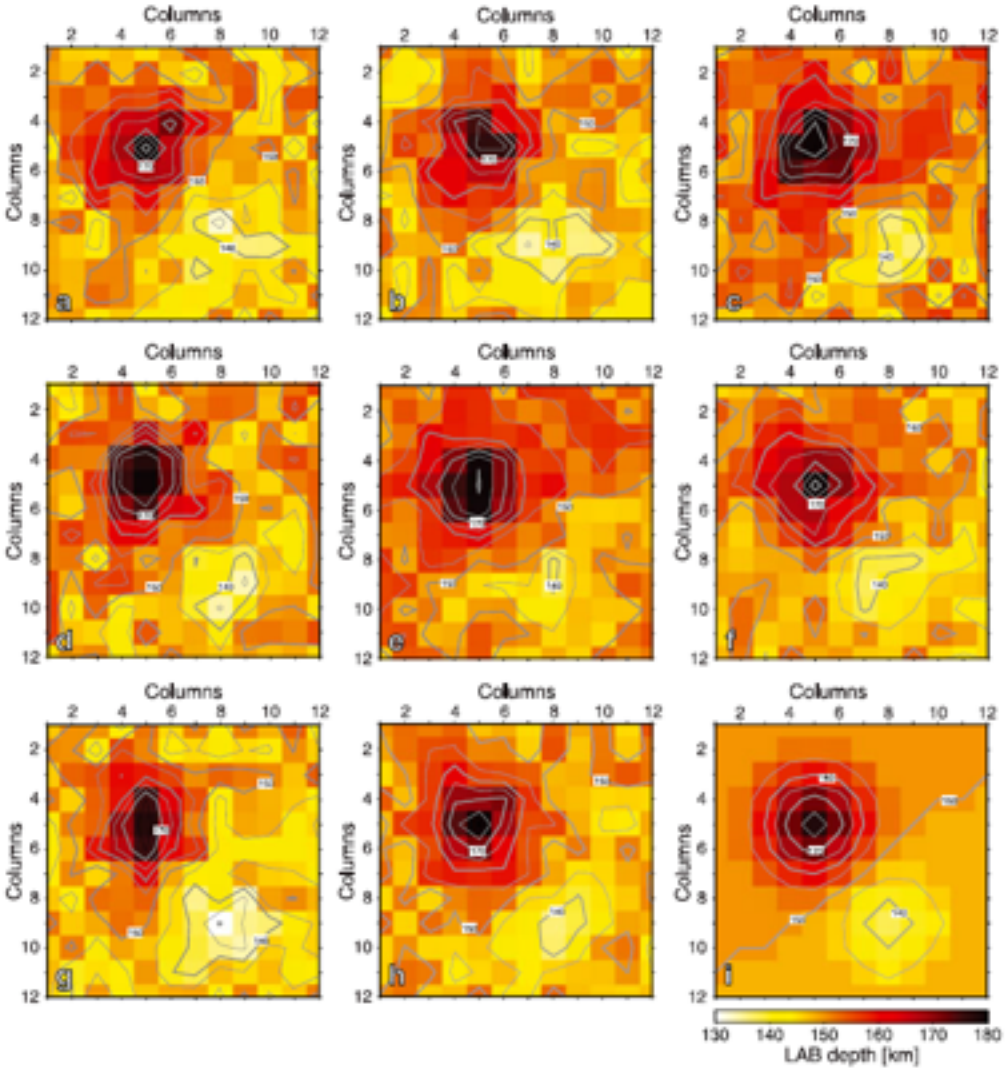

Mean LAB models of eight subsets of 500 random samples taken from the entire collection of acceptable models defining the posterior σ(**m**). The true model is shown for comparison at the bottomright (i). Note that LAB anomalies with amplitudes close to the original values are persistent across all mean maps.

Inverted composition
Mg# number

Christian-Albrechts-Universität zu Kiel

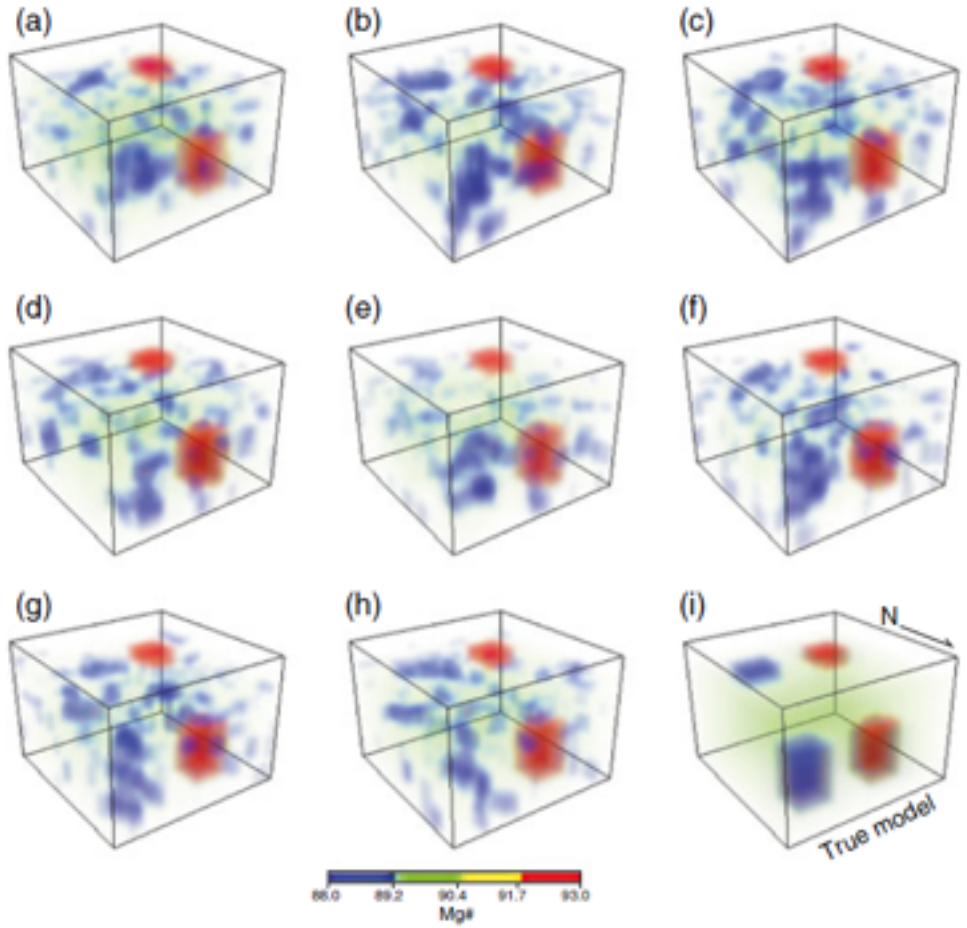

Mean-models of eight subsets of 500 random samples taken from the complete collection of acceptable models defining the posterior PDF. (i) true model.

Inverted composition Al_2O_3 content

Christian-Albrechts-Universität zu Kiel

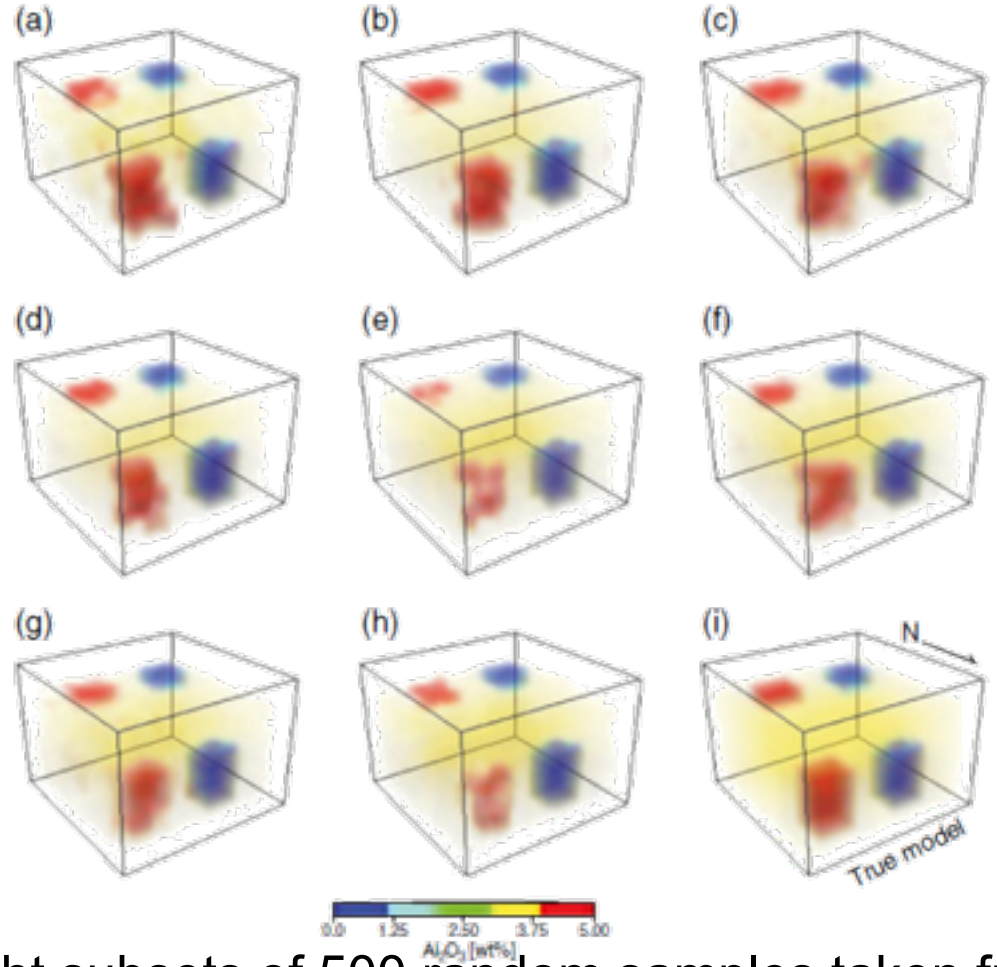

Mean-models of eight subsets of 500 random samples taken from the complete collection of acceptable models defining the posterior PDF. (i) true model.

Sensitivity of inversion

Christian-Albrechts-Universität zu Kiel

The results indicate that only temperature anomalies of T > 150°C and large compositional anomalies of Mg# > 3 (or bulk Al2O3 > 1.5) can be expected to be resolved simultaneously when combining high-quality geophysical data.

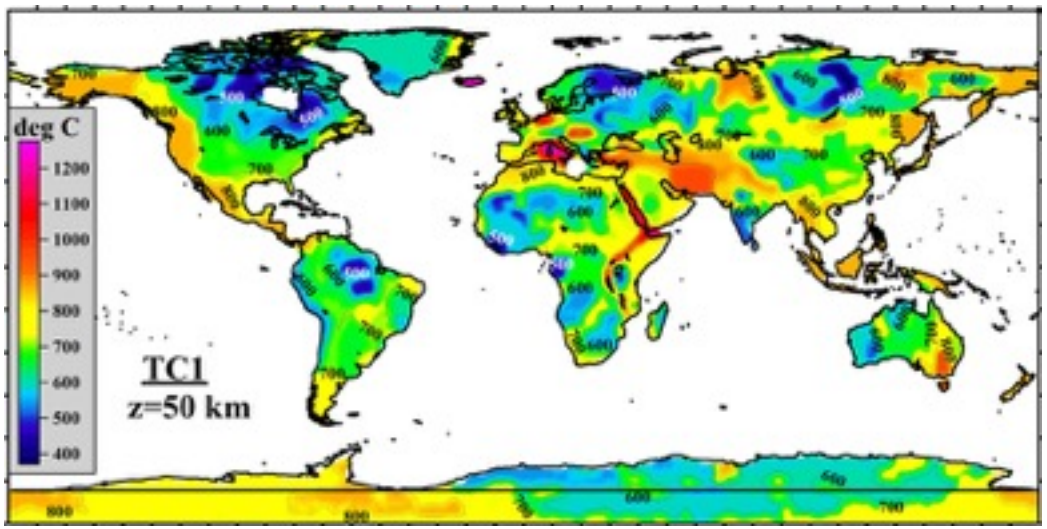

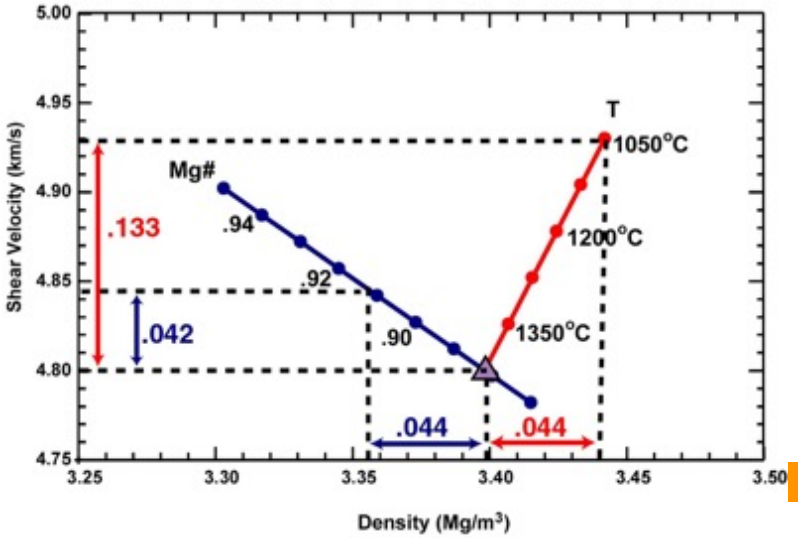

Artemieva 2011

Sensitivity of inversion

Christian-Albrechts-Universität zu Kiel

The results indicate that only temperature anomalies of T > 150°C and large compositional anomalies of Mg# > 3 (or bulk Al2O3 > 1.5) can be expected to be resolved simultaneously when combining high-quality geophysical data.

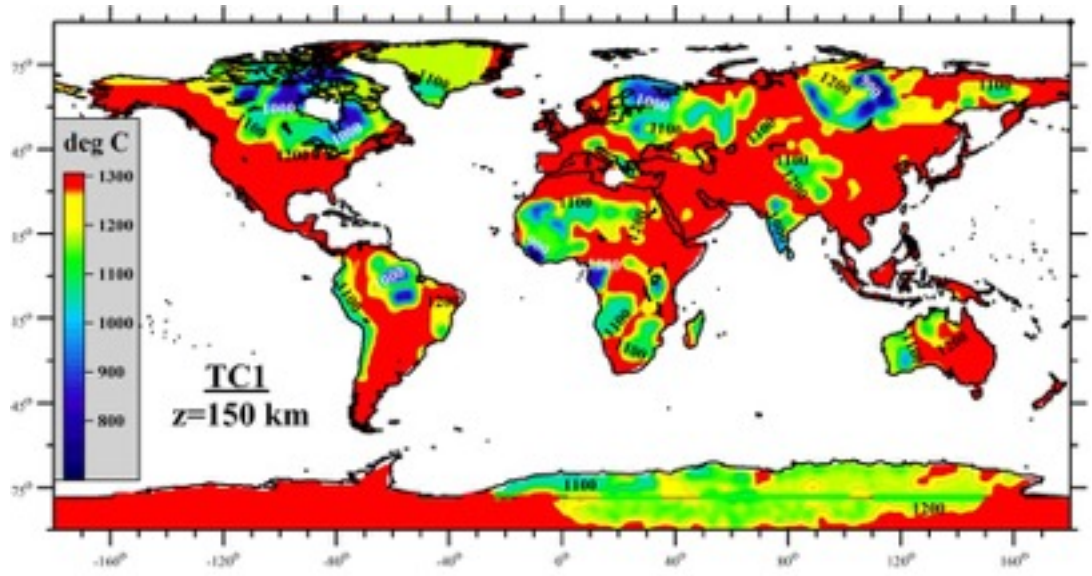

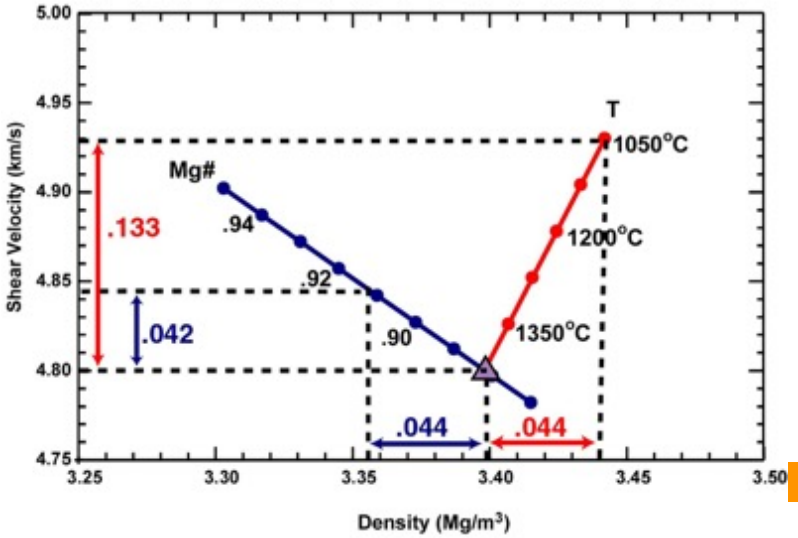

Artemieva 2011

Lithosphere

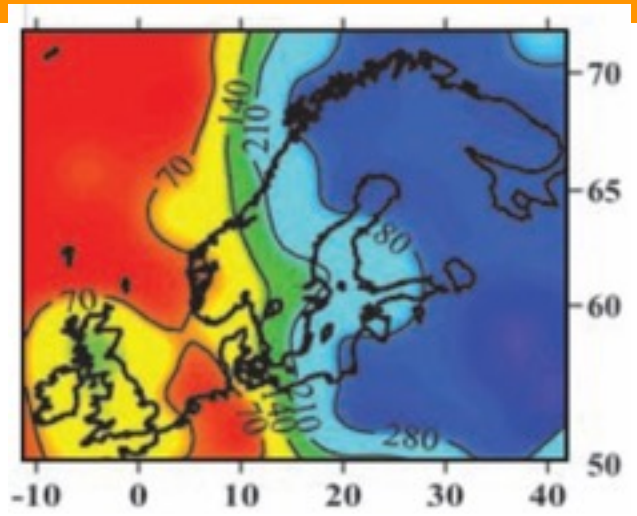

LAB depth

Artemieva & Thybo (2008)

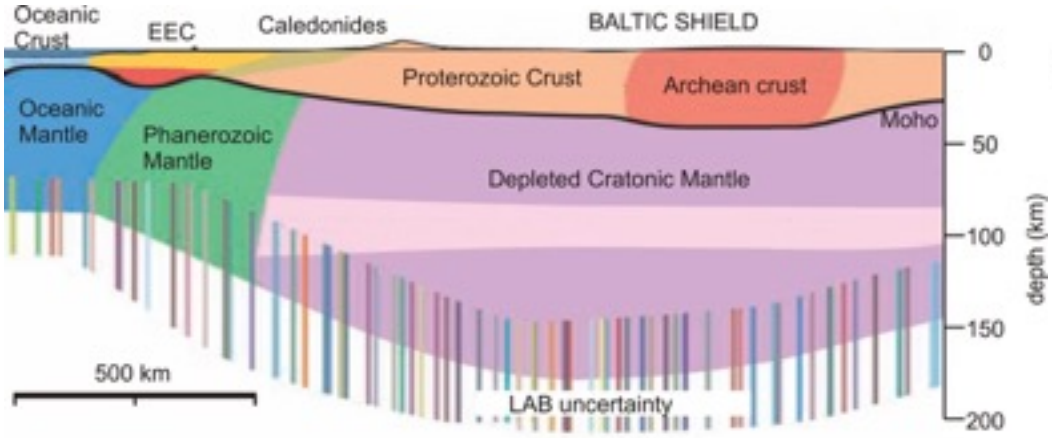

Artemieva & Thybo (2008)

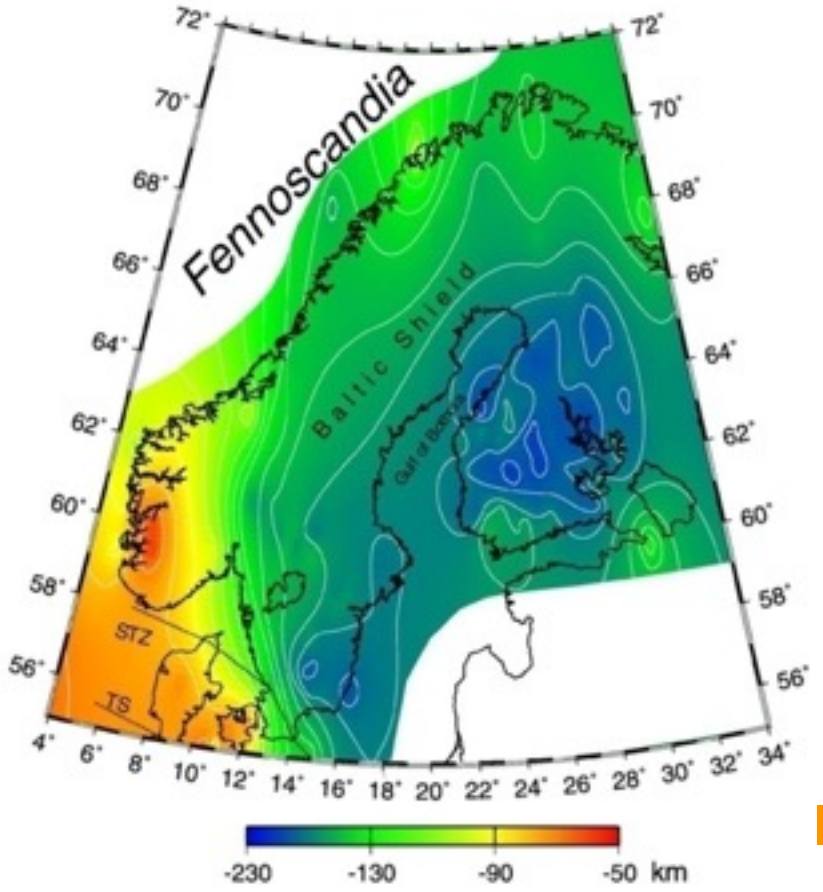

LAB depth

Plomerova et al. (2008)

GOCE -Gravity field and steady-state Ocean Circulation Explorer

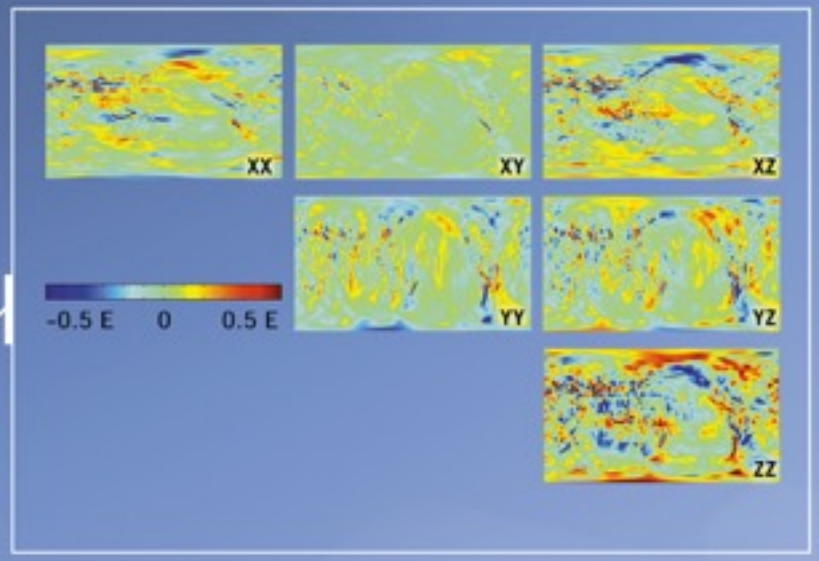

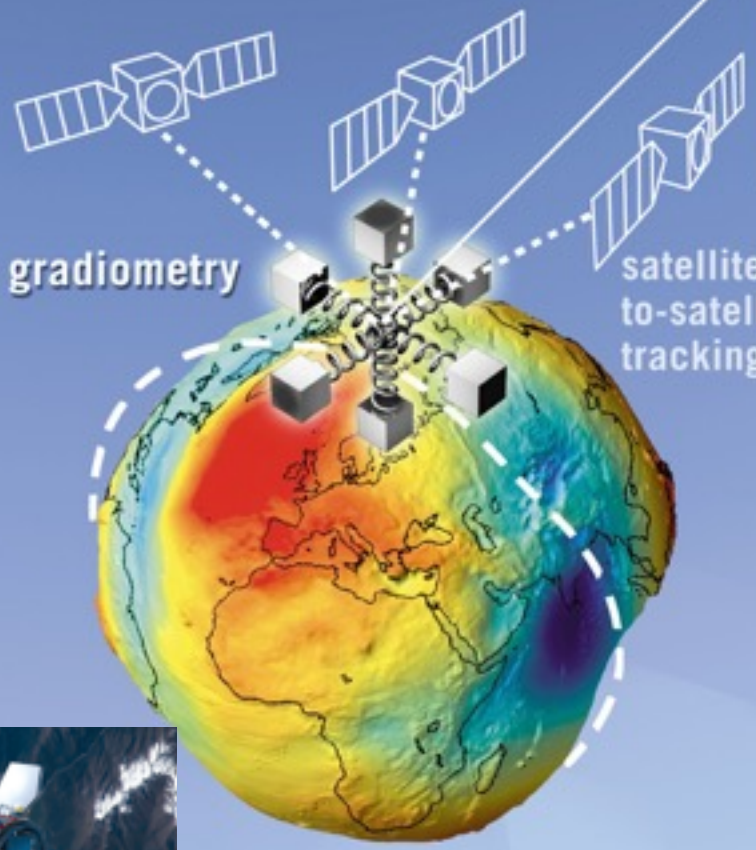

Mission period
17 March 2009 – 11 November 2013

Gradiometer; 3 pairs of 3-axis, servo-controlled, capacitive accelerometers (each pair separated by a distance of about 0.5 m).

Grids can be downloaded from http://goce4interior.dgfi.badw.de

esa support to science element

Gravity gradient grids @ 255 km height

Christian-Albrechts-Universität zu Kiel

North-north

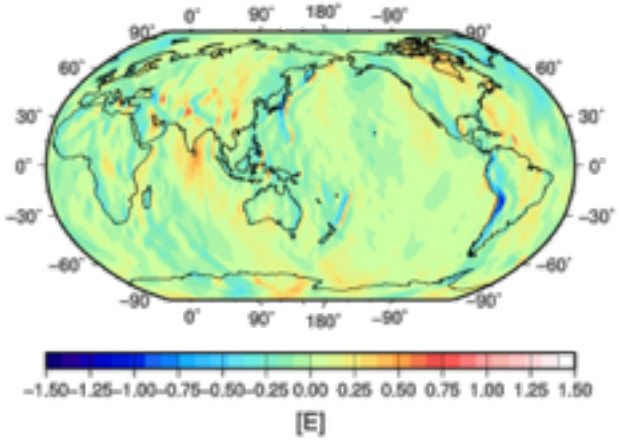

North-east

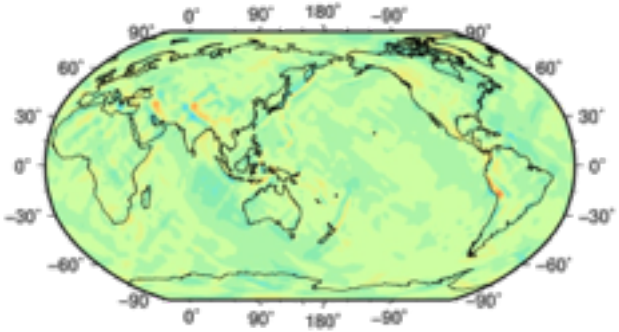

North-radial

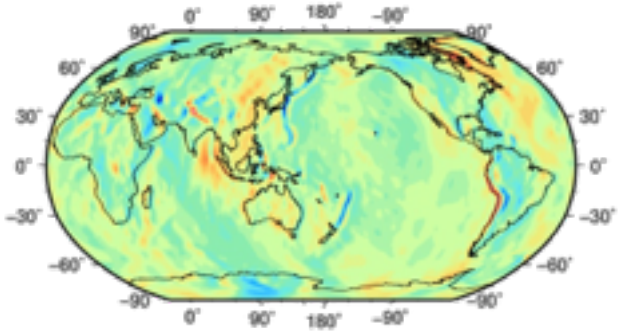

East-east

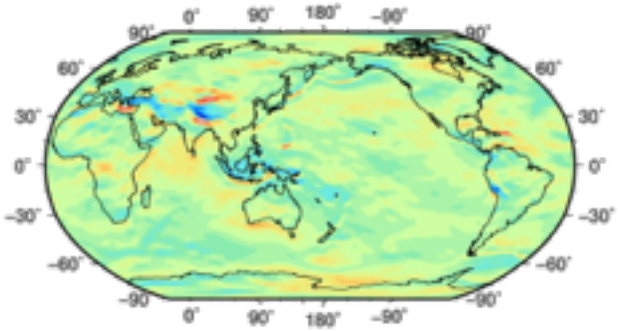

East-radial

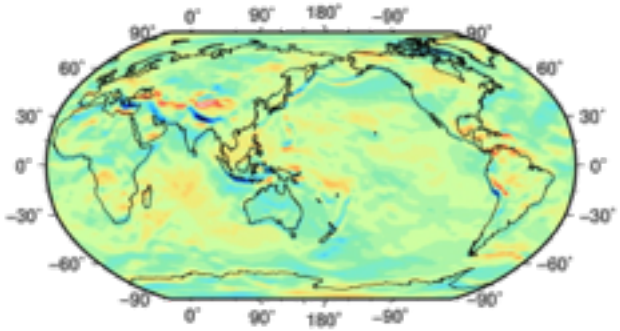

Radial-radial

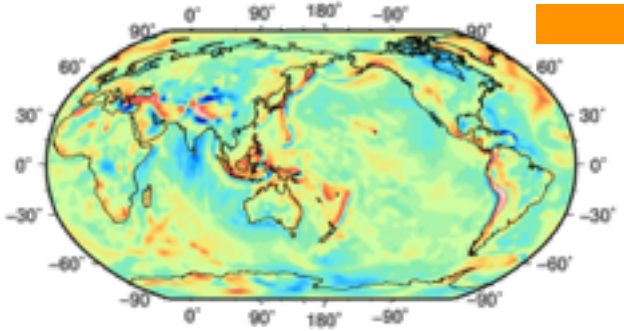

GOCE orbit heights

Christian-Albrechts-Universität zu Kiel

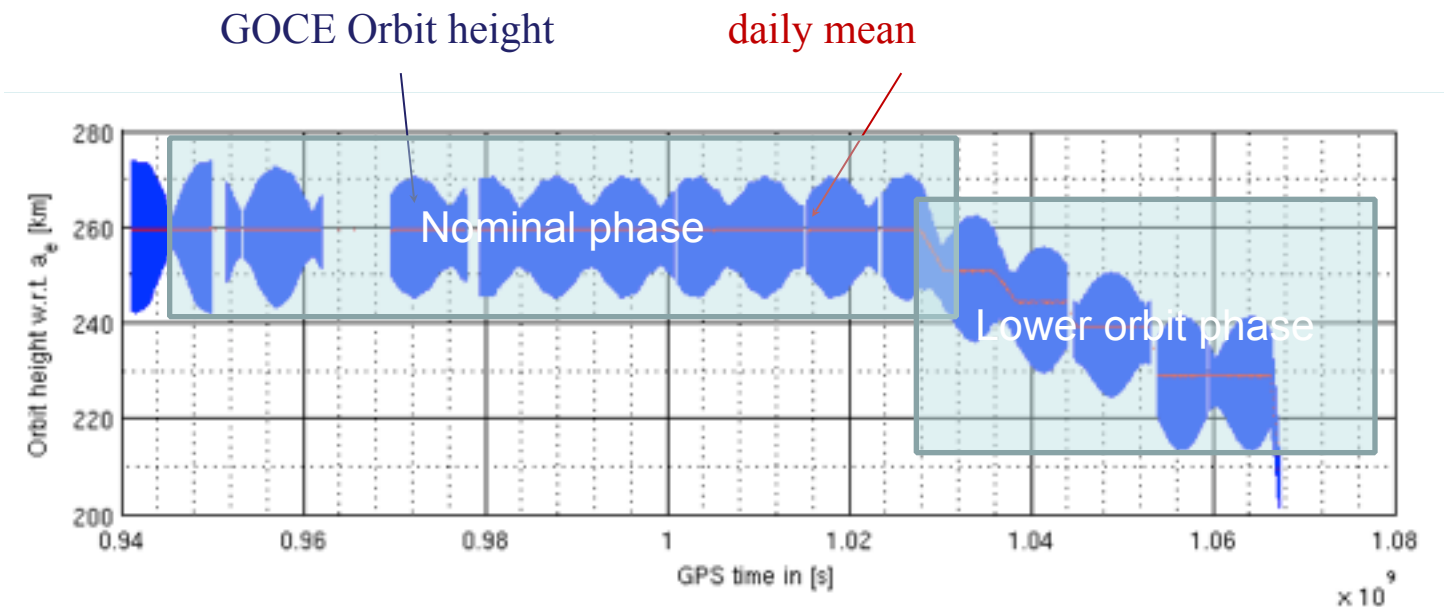

- Four times orbit lowering
  - 30 km Orbit height lowering accounts for approx. 30% signal increase (d/o > 200)
- Nominal phase had perigee height of 255 km
- Lower orbit phase had perigee height of 225 km

GOCE data @ satellite altitude / Earth's surface

Christian-Albrechts-Universität zu Kiel

- Downward continuation also amplifies noise
- Effective resolution of data does not change
- Omission error becomes much larger (mainly high frequency topography)

V_{zz} degree RMS h = 0 & 260 km

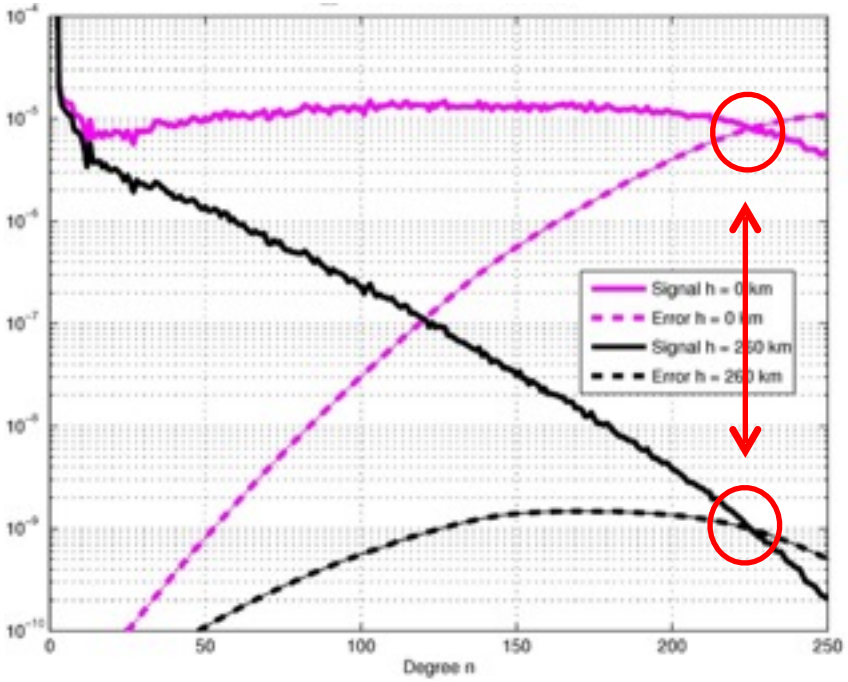

GOCO03S V_{zz} signal & error, L = 225

Saudi Arabia	Height		
	0 km	10 km	260 km
Signal RMS	5.1 E	4.1 E	0.3 E
Model error	1.3 E	0.9 E	0.4 mE

For model inversion it is probably best to use data close to their original point of acquisition.

Lithospheric model set-up

Christian-Albrechts-Universität zu Kiel

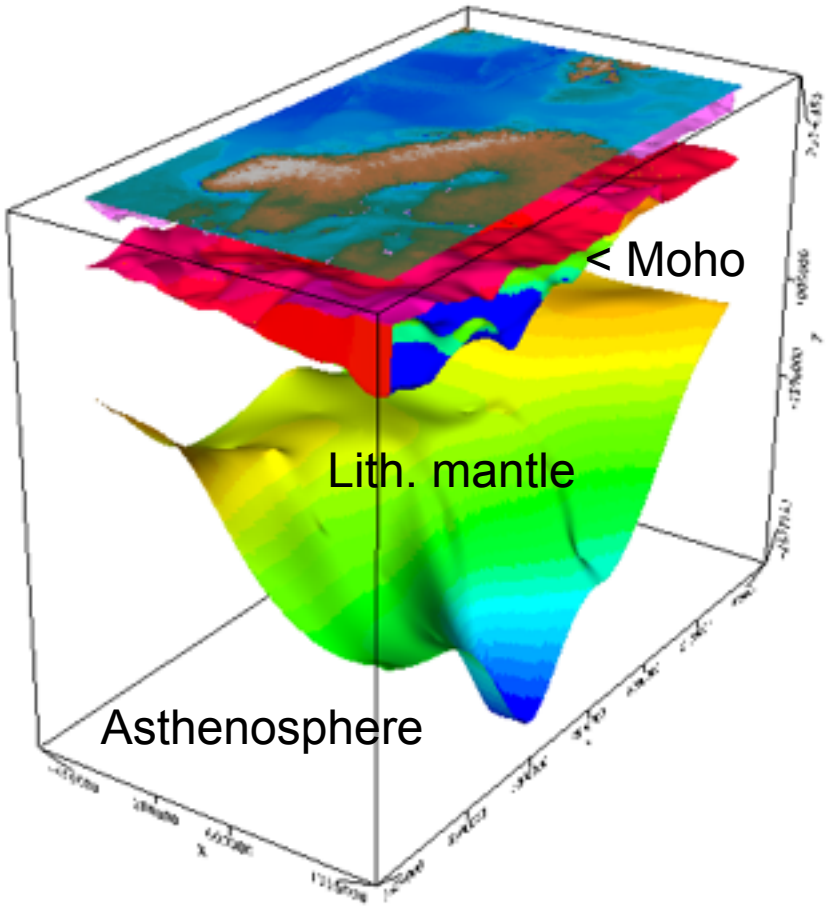

- Model Name: 3D_NEAtlantic.g3d
- Global Information
- Vertical Density Function
- Gravity
- Magnetic
- Layer 1: .\3DMod_Topography10.grd(GRD)
  - Density: 2.67
  - Susc: Constant
- Layer 2: .\Null10.grd(GRD)
  - Density: 1.03
  - Susc: Constant
- Layer 3: .\3DMod_Bathymetry10.grd(GRD)
  - Density: Vertical Density Function
  - Susc: Constant
- Layer 4: .\BaseSed_NGU_NOAA_Laske.grd
  - Density: .\D_UC1.grd
  - Susc: Constant
- Layer 5: .\UCMC.grd
  - Density: 2.8
  - Susc: Constant
- Layer 6: .\UCLC.grd
  - Density: 2.95
  - Susc: Constant
- Layer 7: .\3DMod_IsoTopLCBClipped.grd(GRD)
  - Density: 3.1
  - Susc: Constant
- Layer 8: .\3DMod_Moho_Grad.grd
  - Density: .\MantleDensityGP250km.grd
  - Susc: Constant
- Layer 9: .\LAB_Artemieva2.grd
  - Density: 3.3

Relative signal power @225 km height

Christian-Albrechts-Universität zu Kiel

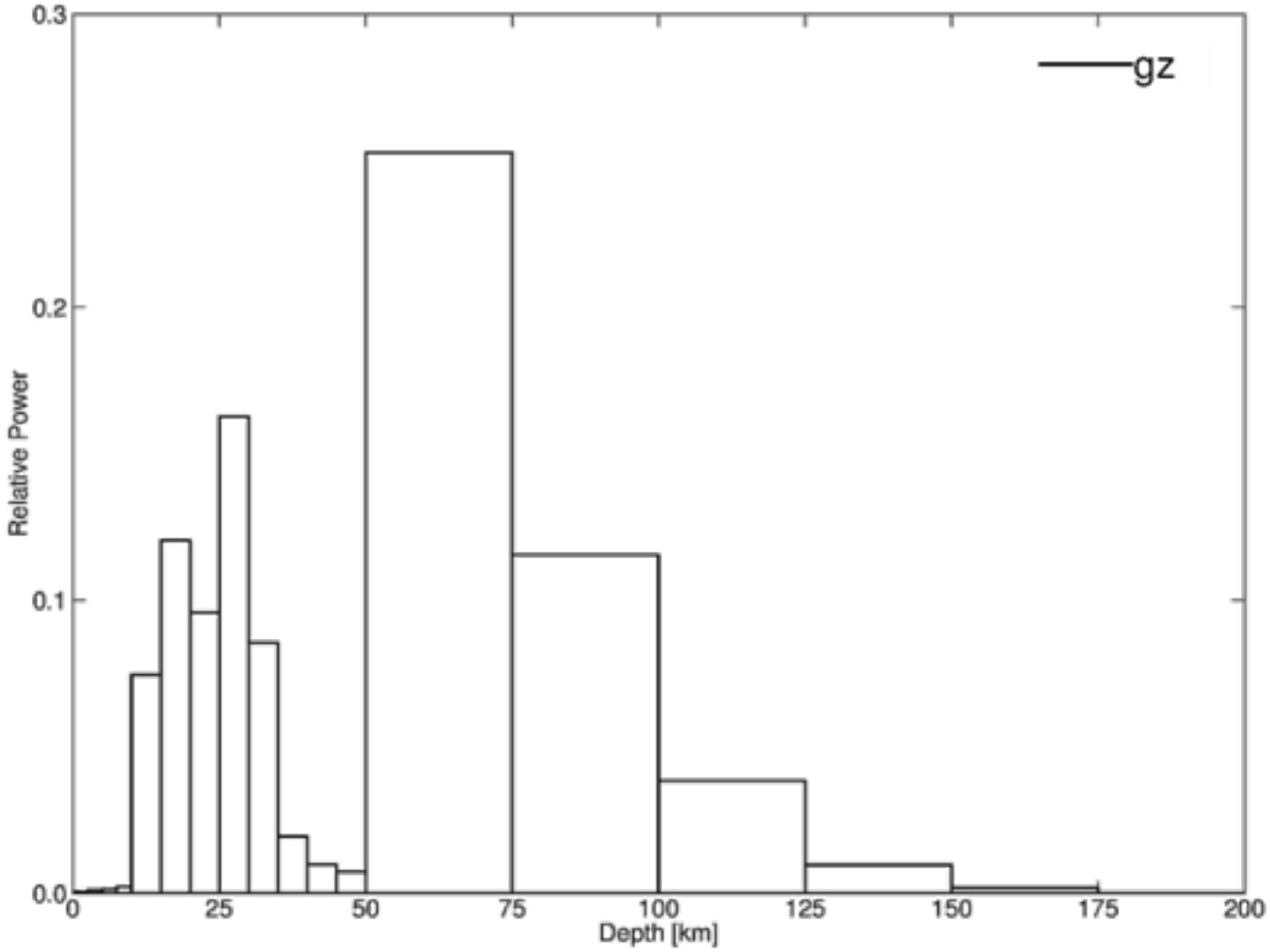

Relative signal power @225 km height

Christian-Albrechts-Universität zu Kiel

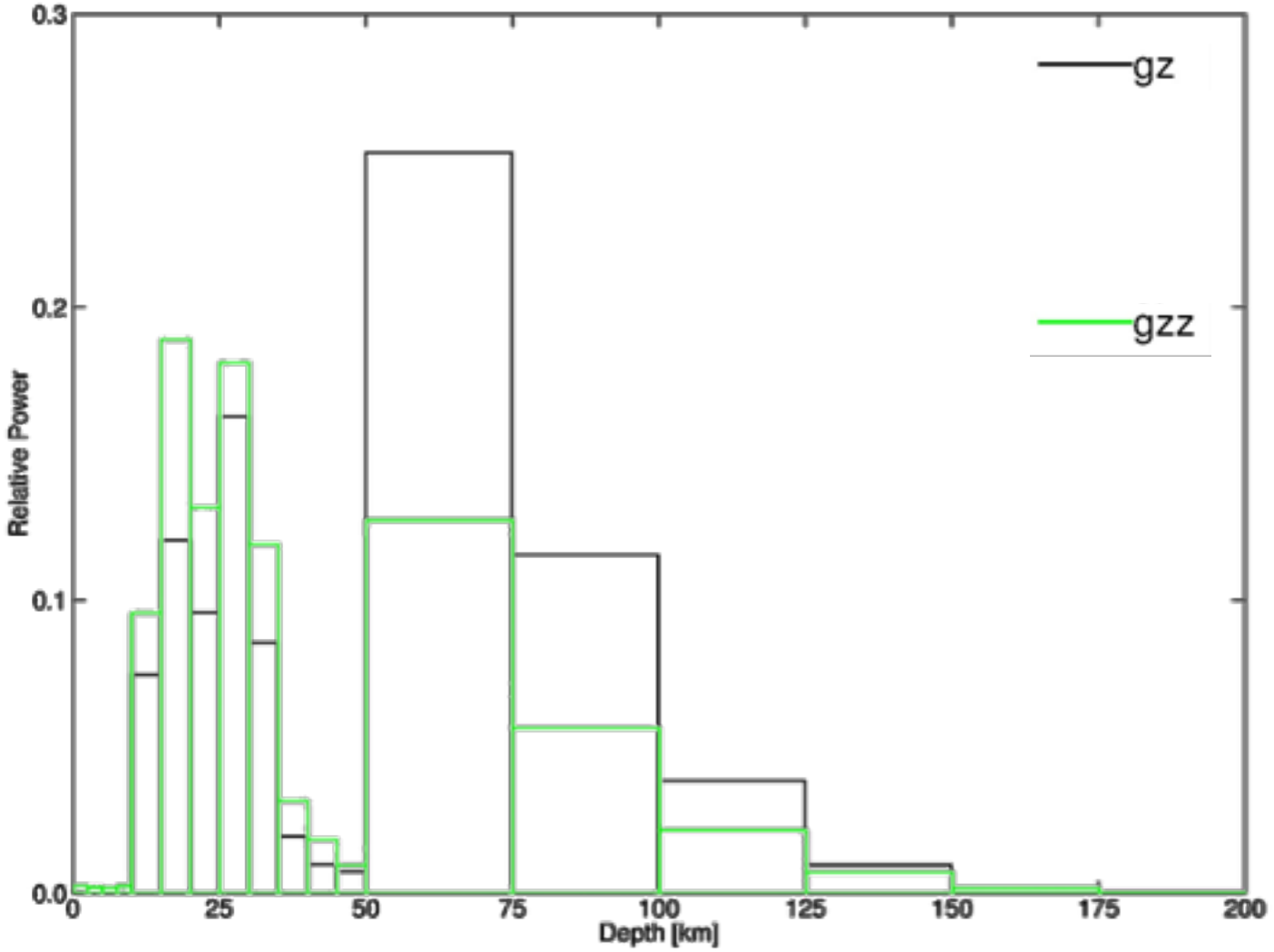

Relative signal power @225 km height

Christian-Albrechts-Universität zu Kiel

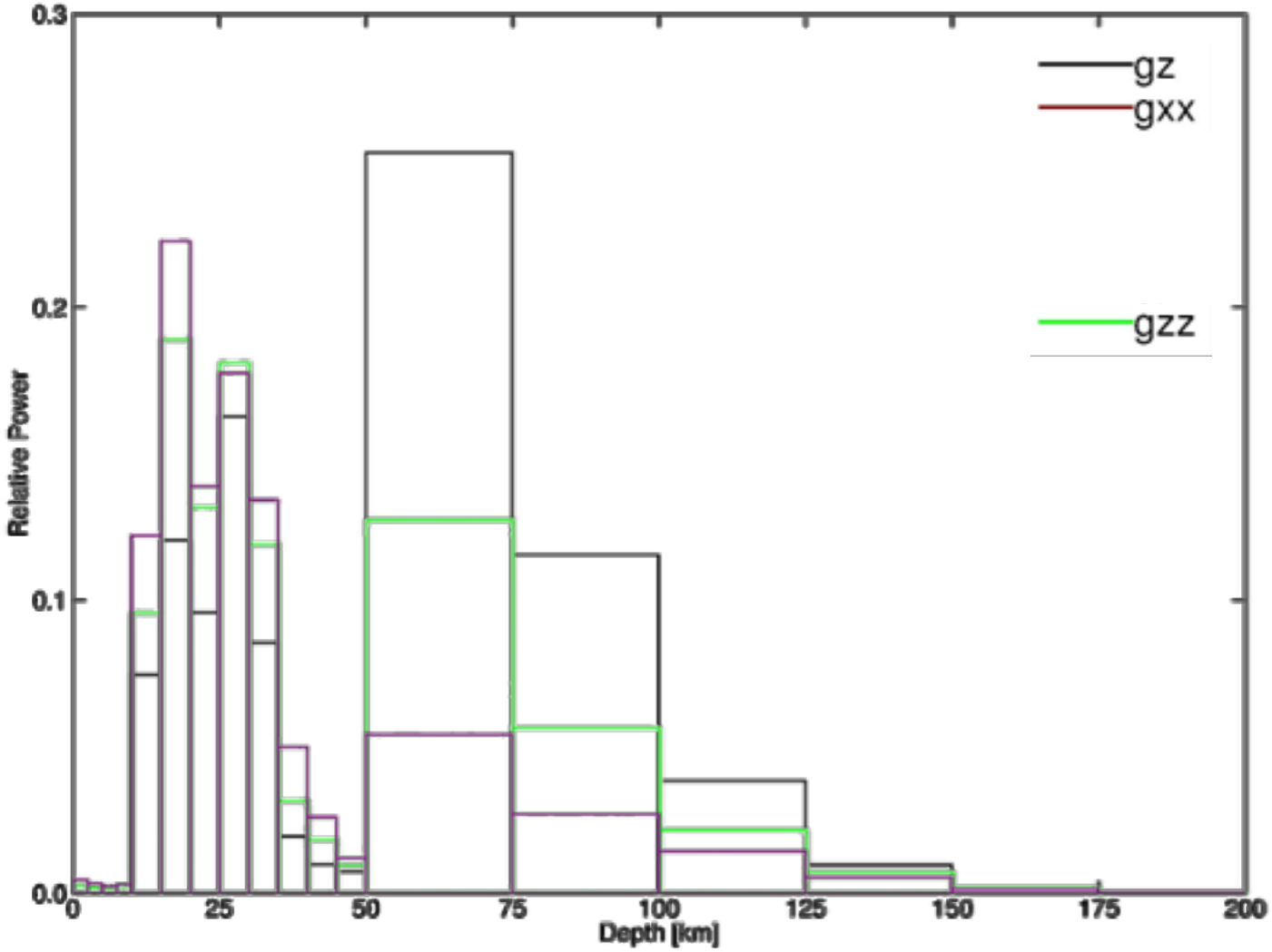

Relative signal power @225 km height

Christian-Albrechts-Universität zu Kiel

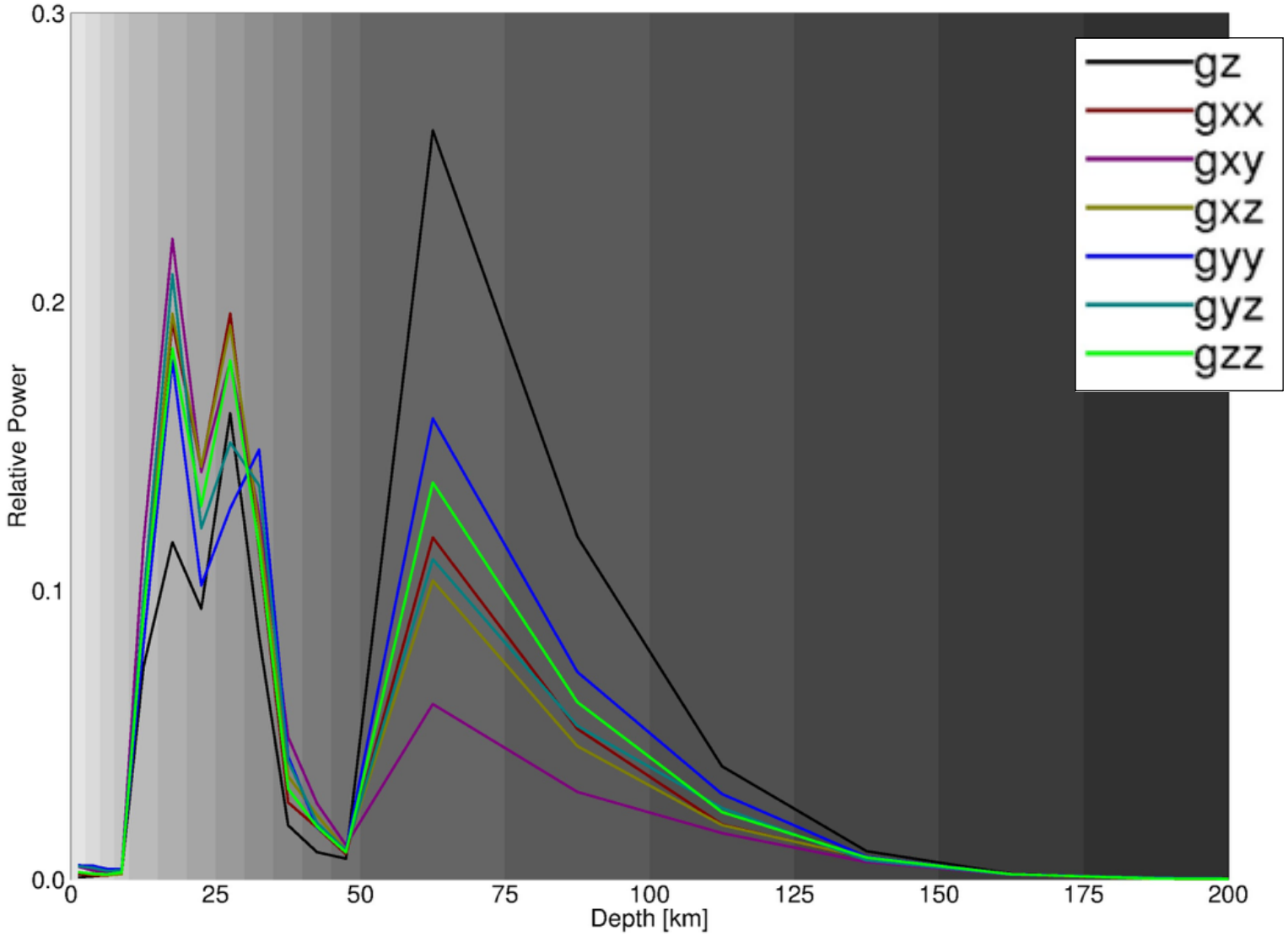

Comparison to global tomography

Christian-Albrechts-Universität zu Kiel

Vs

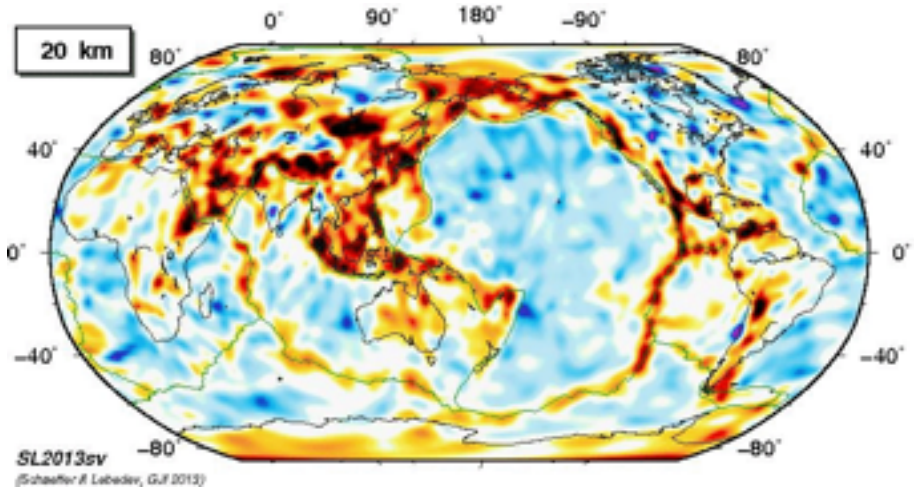

North-east@225km

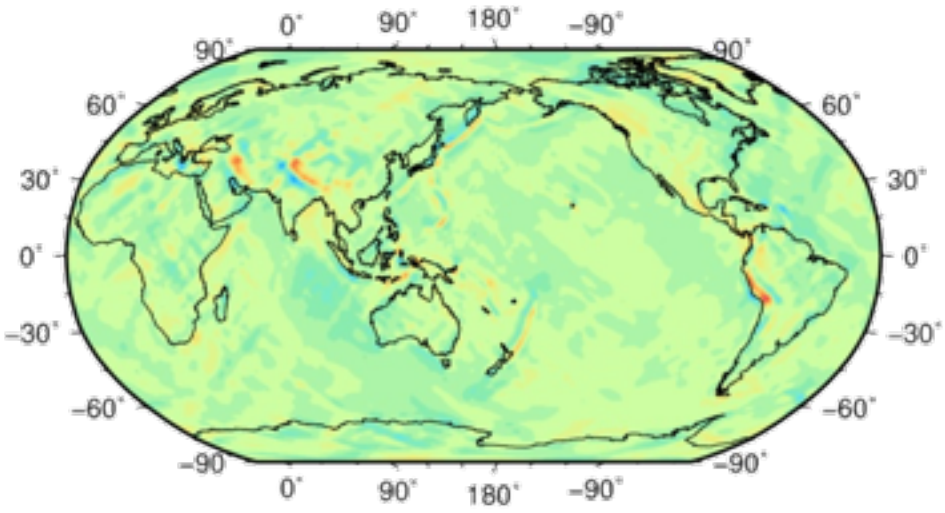

Radial@225km

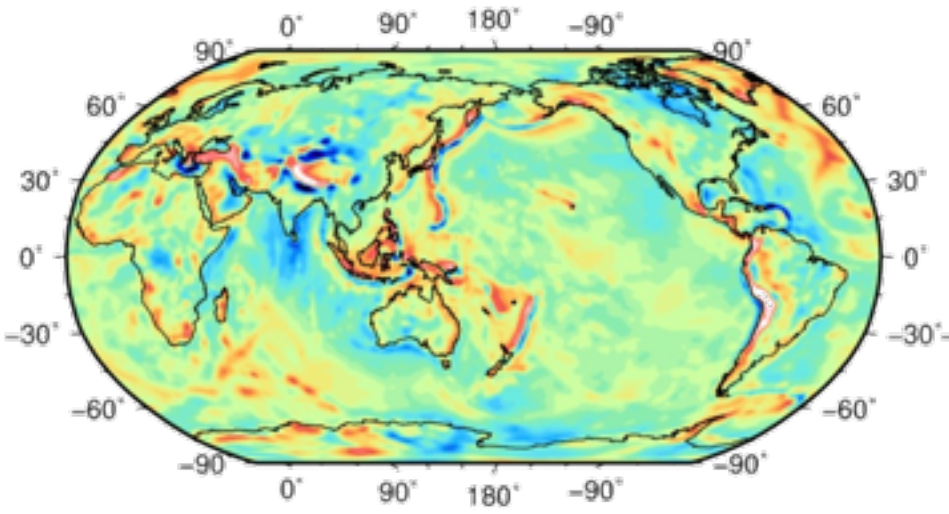

North-radial@225km

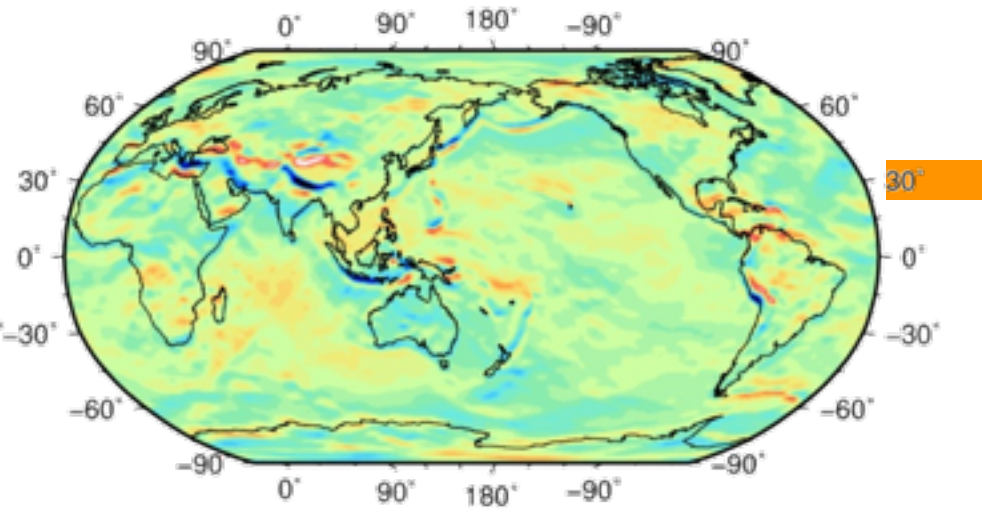

Comparison to global tomography

Christian-Albrechts-Universität zu Kiel

Vs

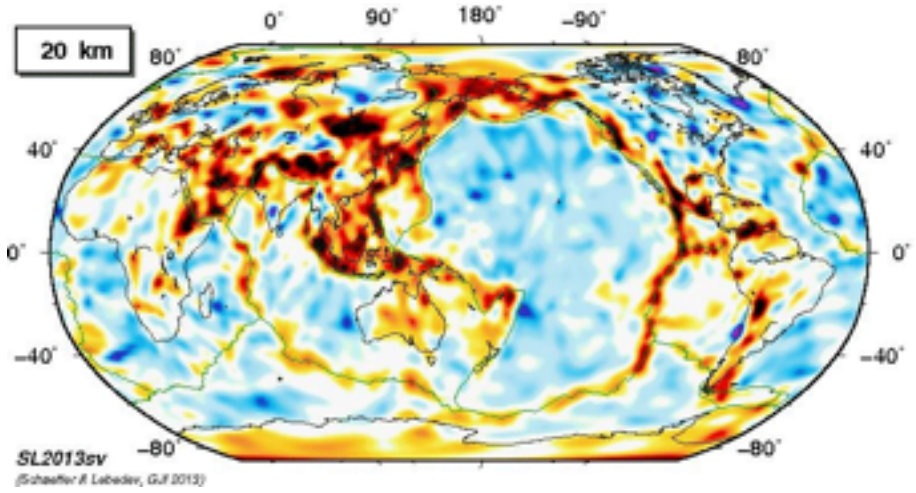

North-east@225km

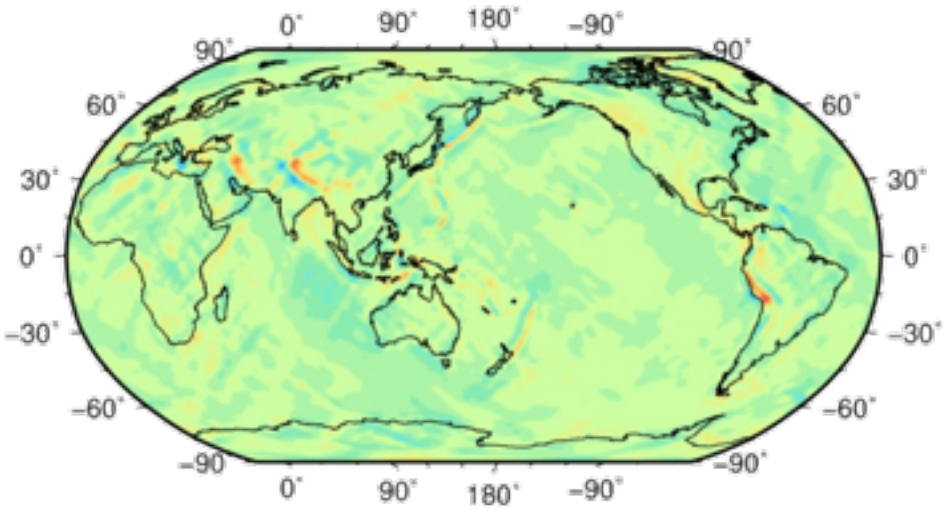

Radial@225km

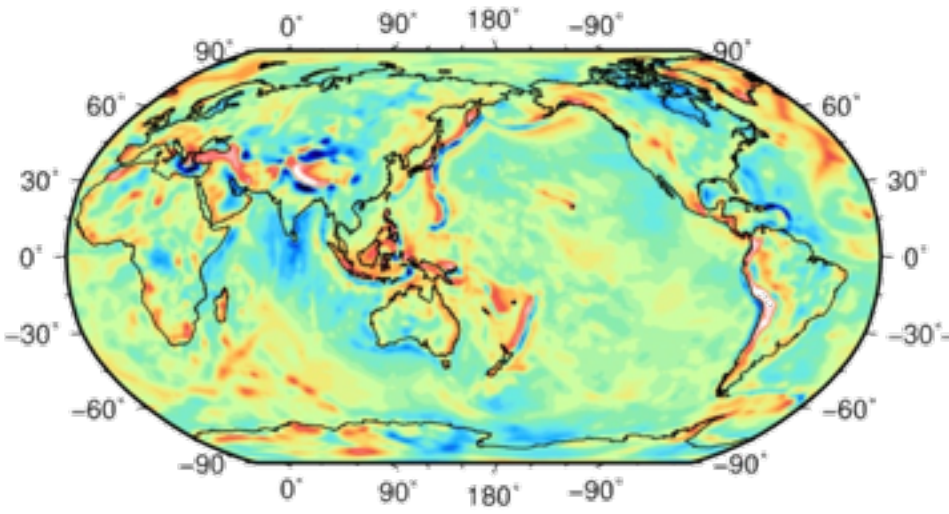

North-radial@225km

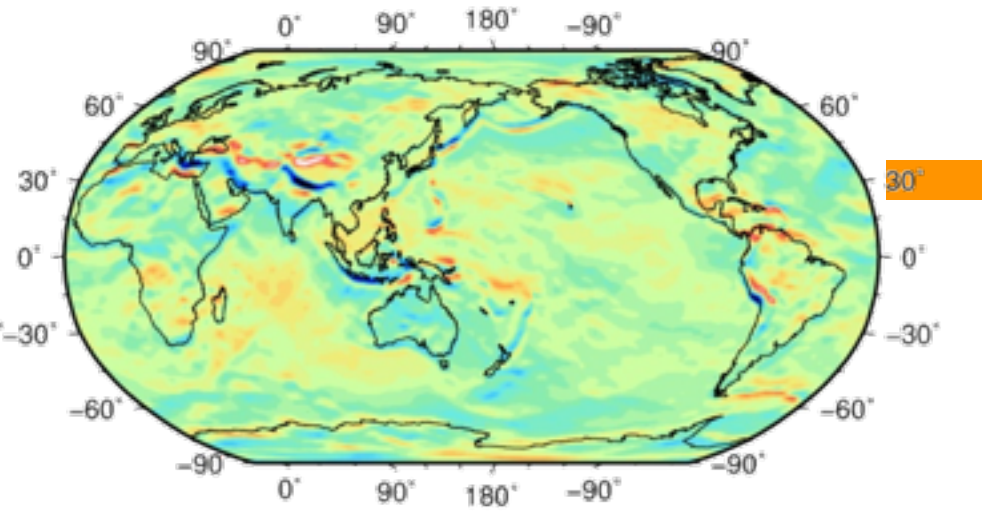

Comparison to tomography
Gradient Tensor: Depth 50 km

Christian-Albrechts-Universität zu Kiel

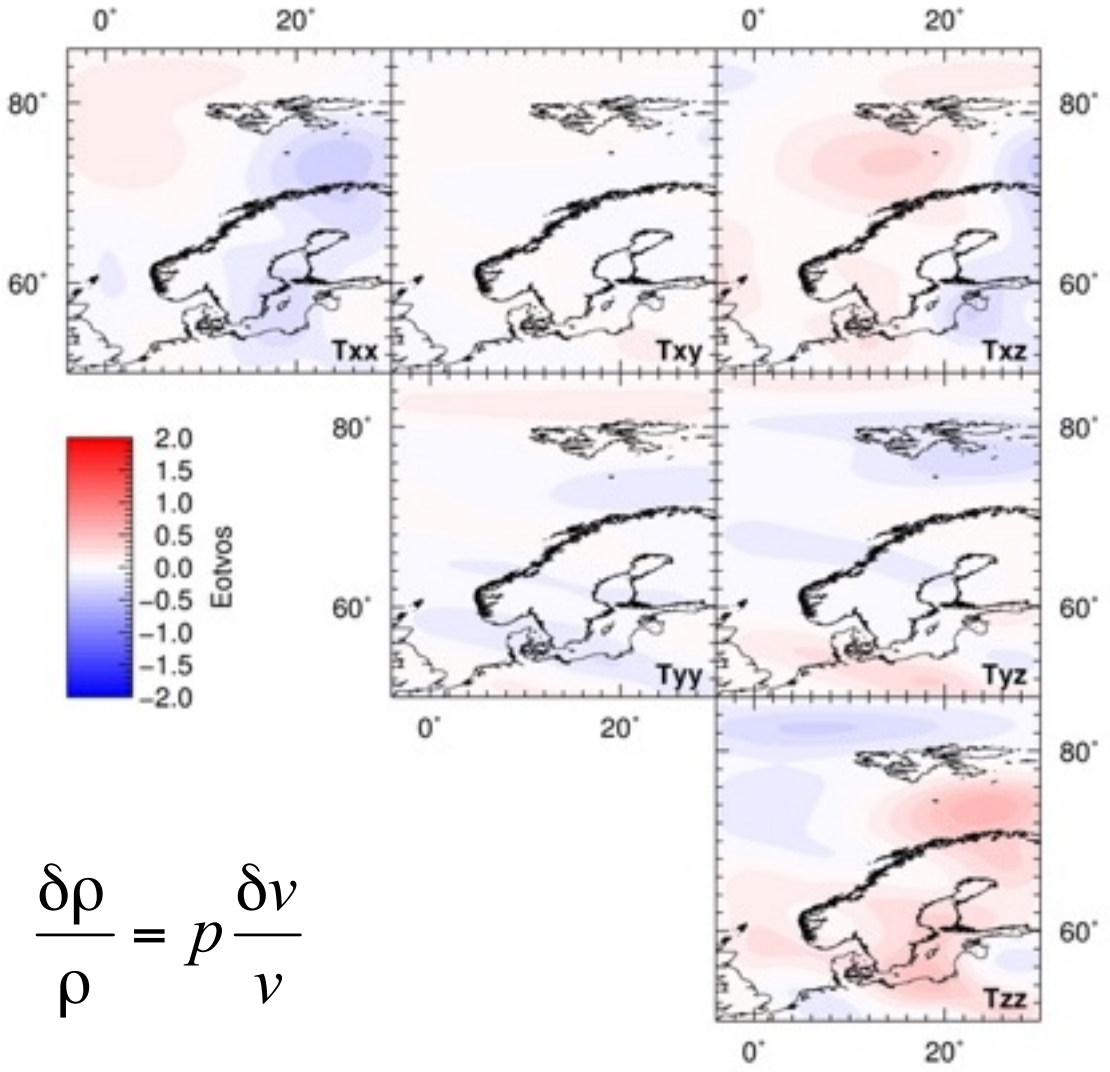

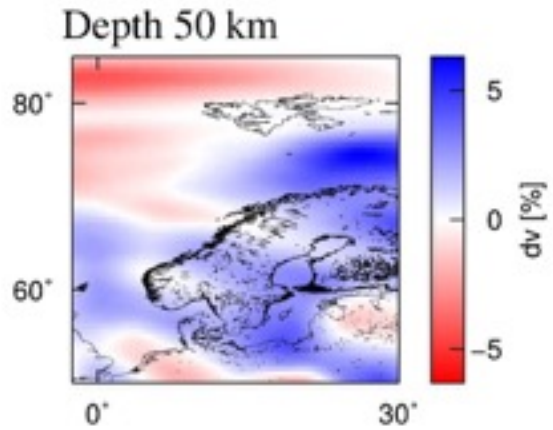

$$\frac{\delta\rho}{\rho} = p\frac{\delta v}{v}$$

Comparison to tomography
Gradient Tensor: Depth 75 km

Christian-Albrechts-Universität zu Kiel

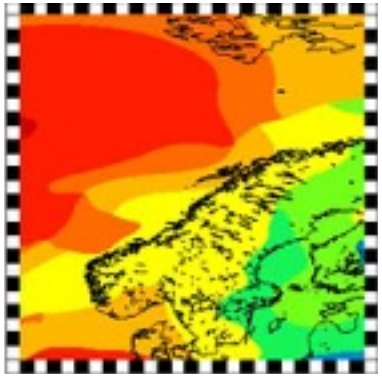

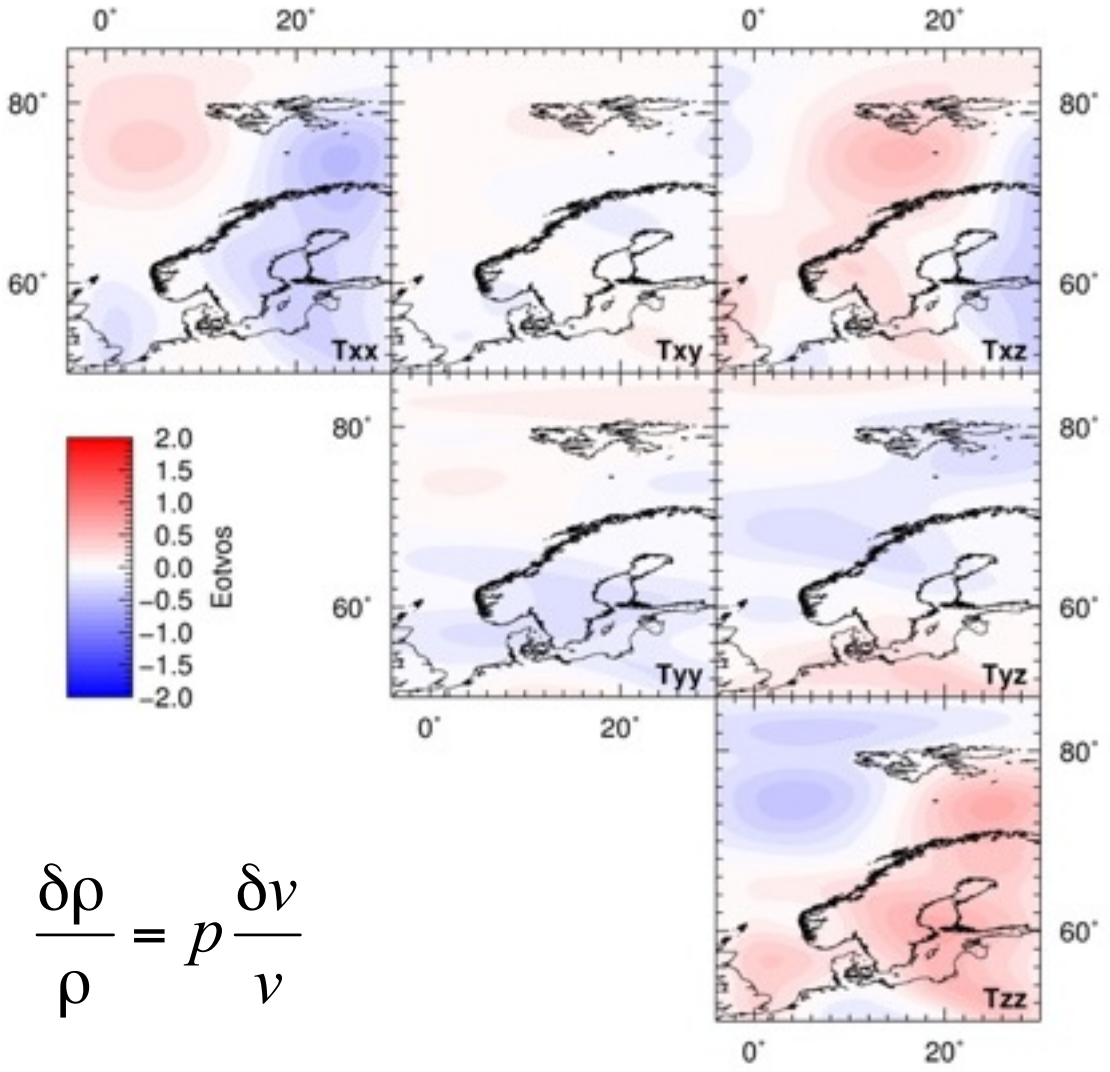

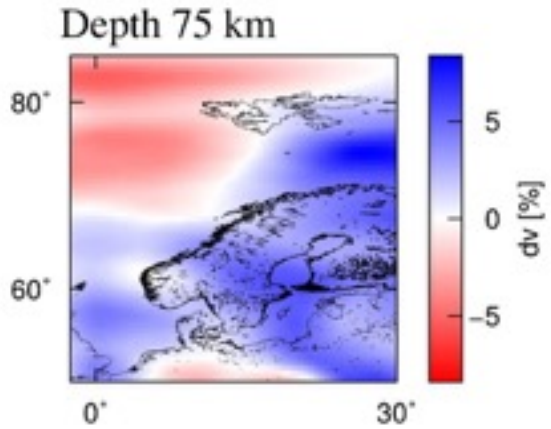

$$\frac{\delta\rho}{\rho} = p\frac{\delta v}{v}$$

Comparison to tomography
Gradient Tensor: Depth 100 km

Christian-Albrechts-Universität zu Kiel

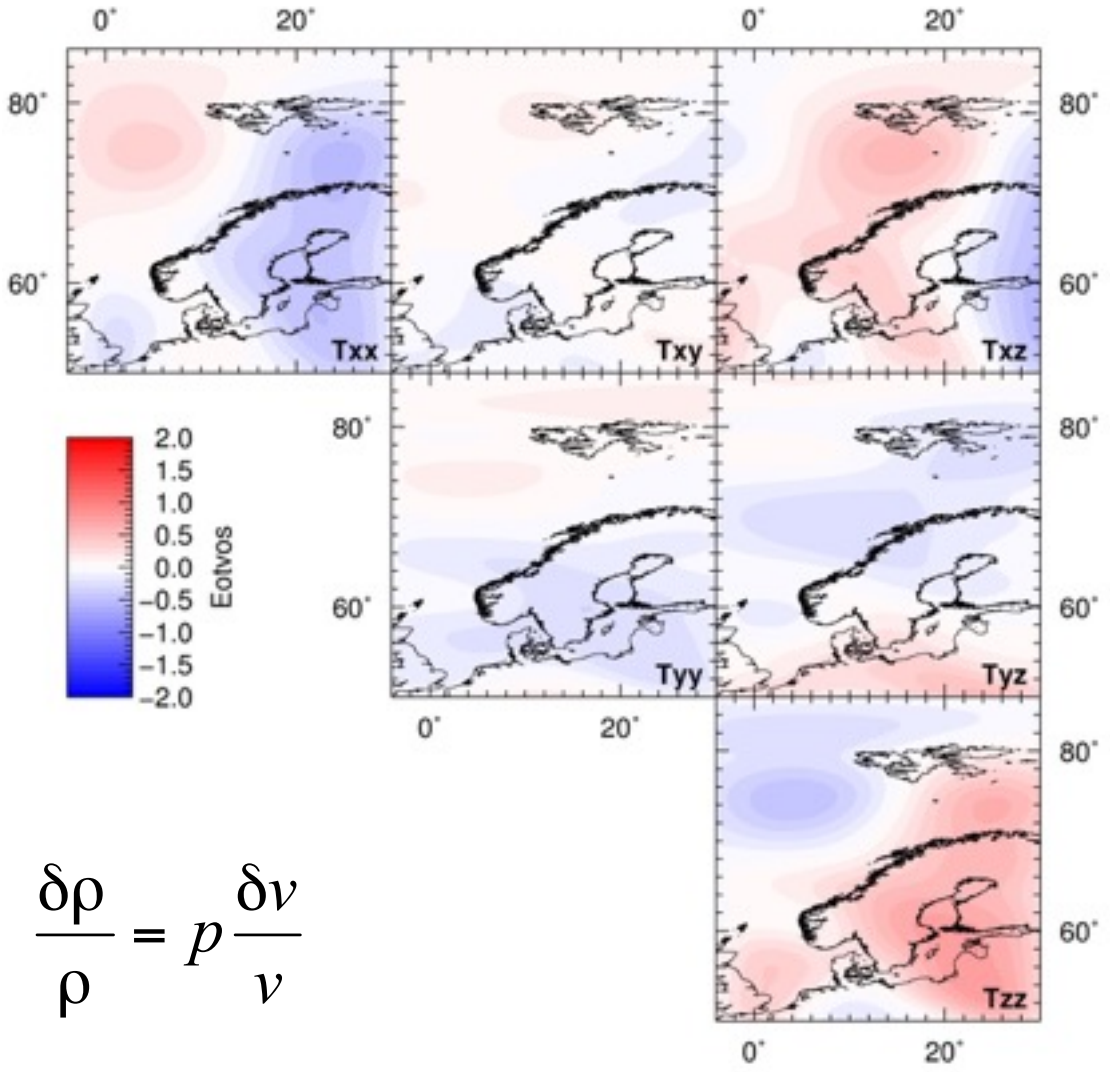

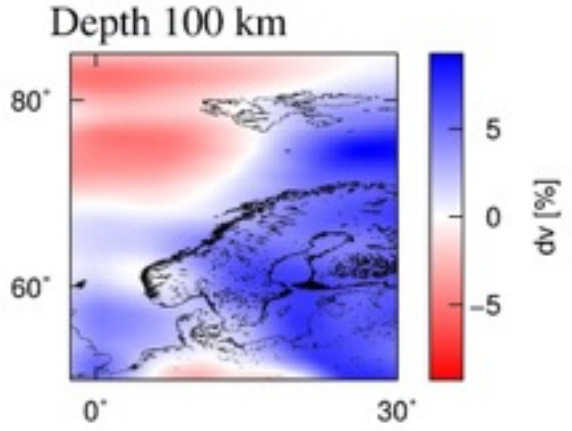

$$\frac{\delta\rho}{\rho} = p\frac{\delta v}{v}$$

Comparison to tomography
Gradient Tensor: Depth 125 km

Christian-Albrechts-Universität zu Kiel

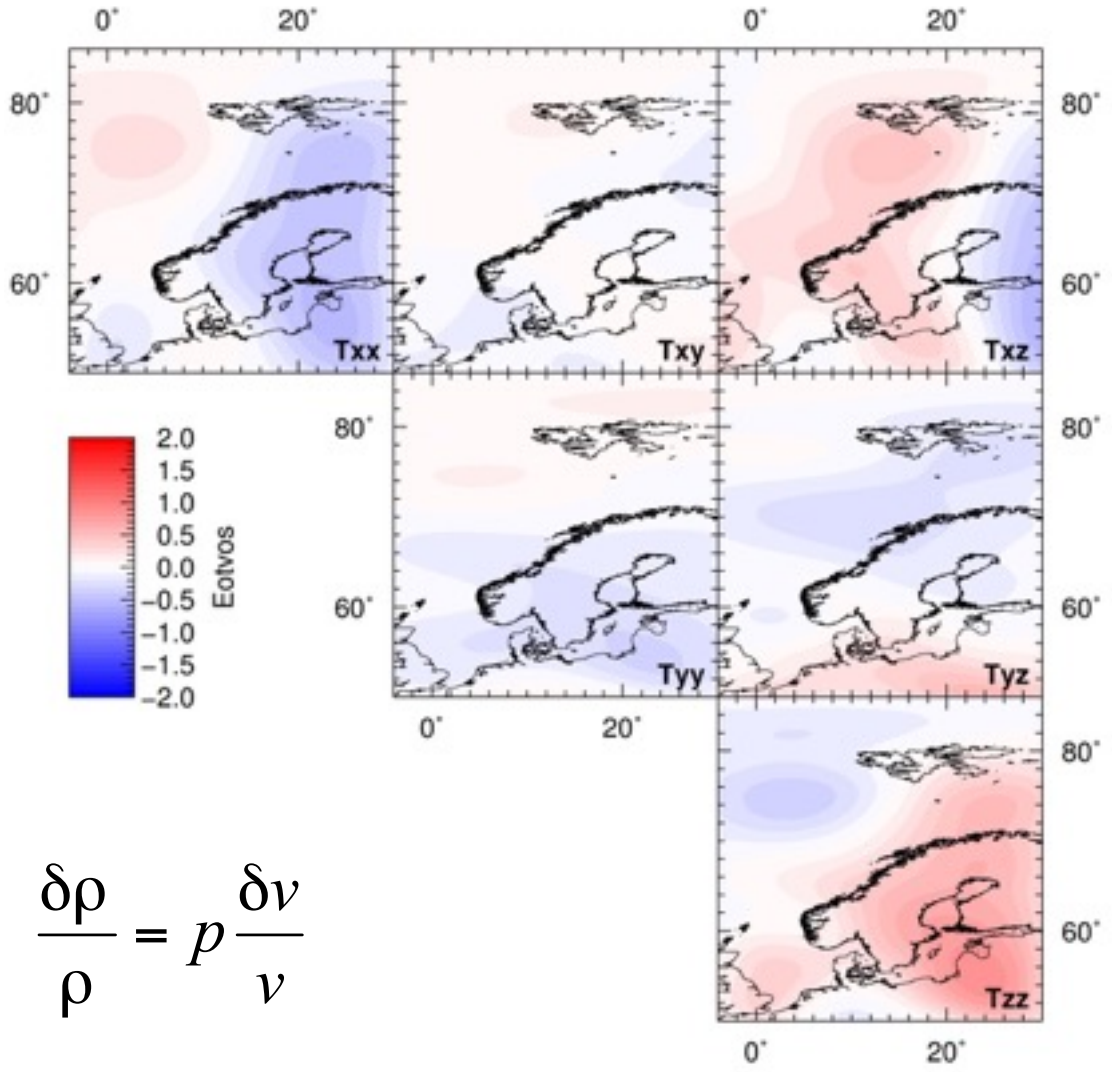

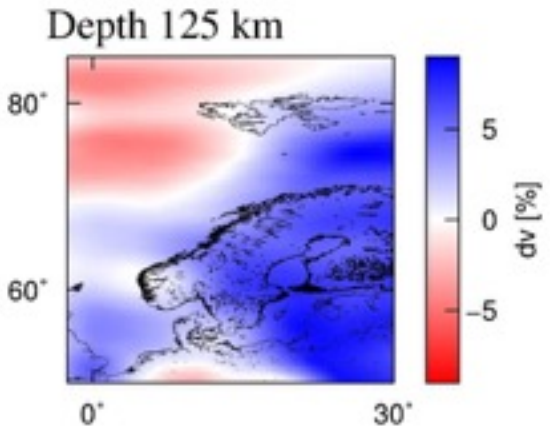

$$\frac{\delta\rho}{\rho} = p\frac{\delta v}{v}$$

Comparison to tomography
Gradient Tensor: Depth 150 km

Christian-Albrechts-Universität zu Kiel

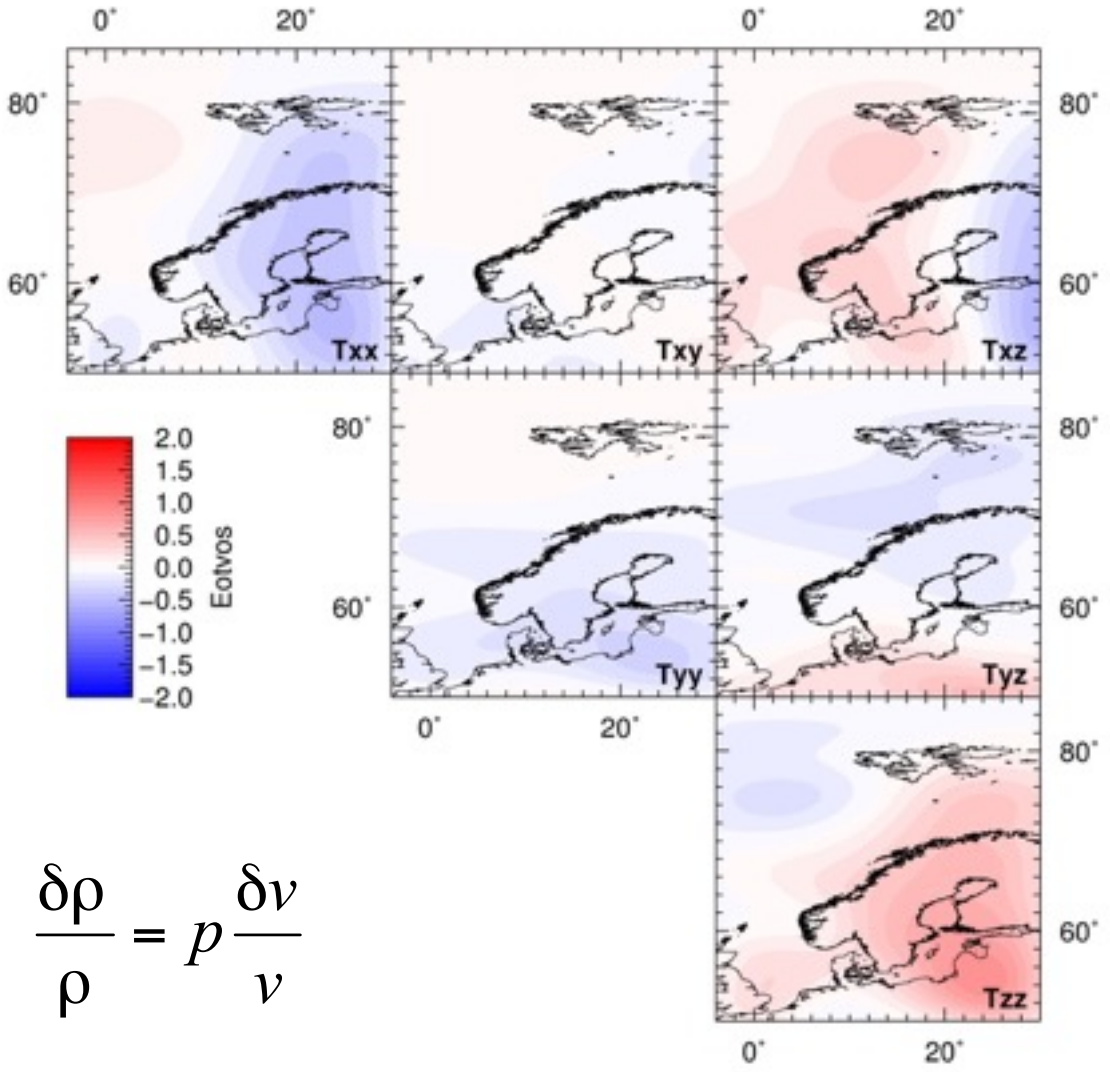

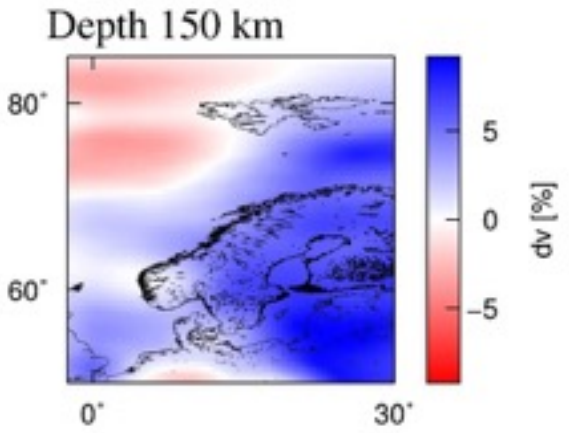

$$\frac{\delta\rho}{\rho} = p\frac{\delta v}{v}$$

Comparison to tomography
Gradient Tensor: Depth 175 km

Christian-Albrechts-Universität zu Kiel

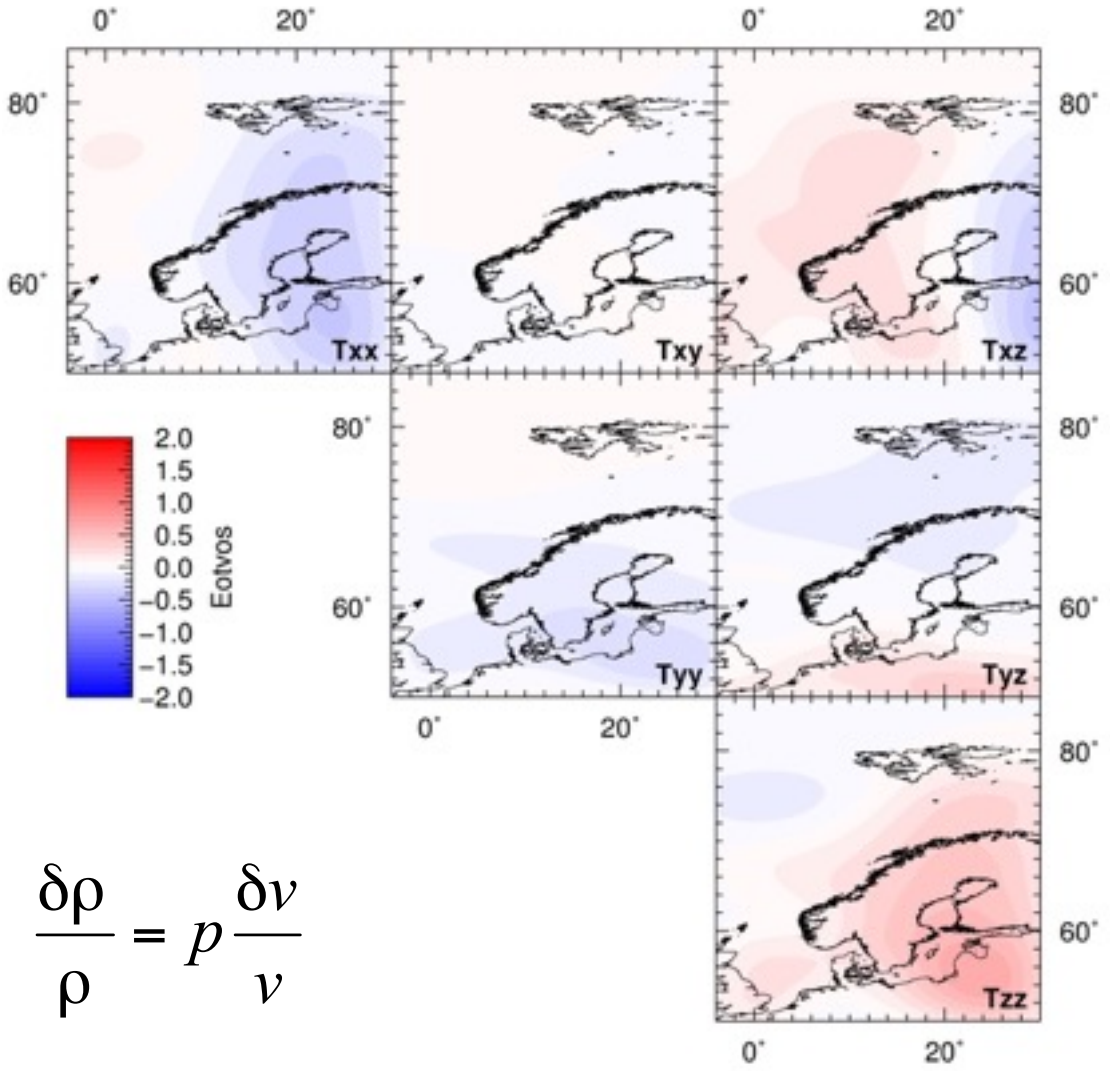

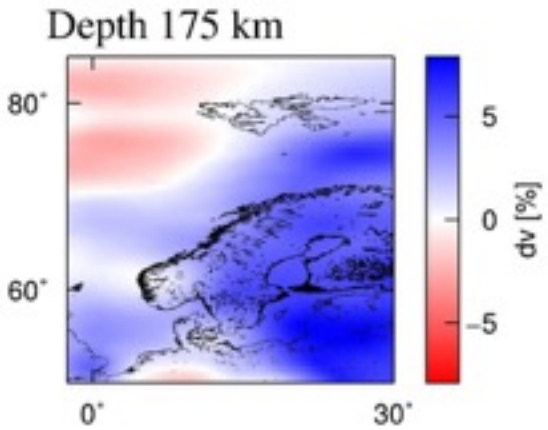

$$\frac{\delta\rho}{\rho} = p\frac{\delta v}{v}$$

Comparison to tomography
Gradient Tensor: Depth 200 km

Christian-Albrechts-Universität zu Kiel

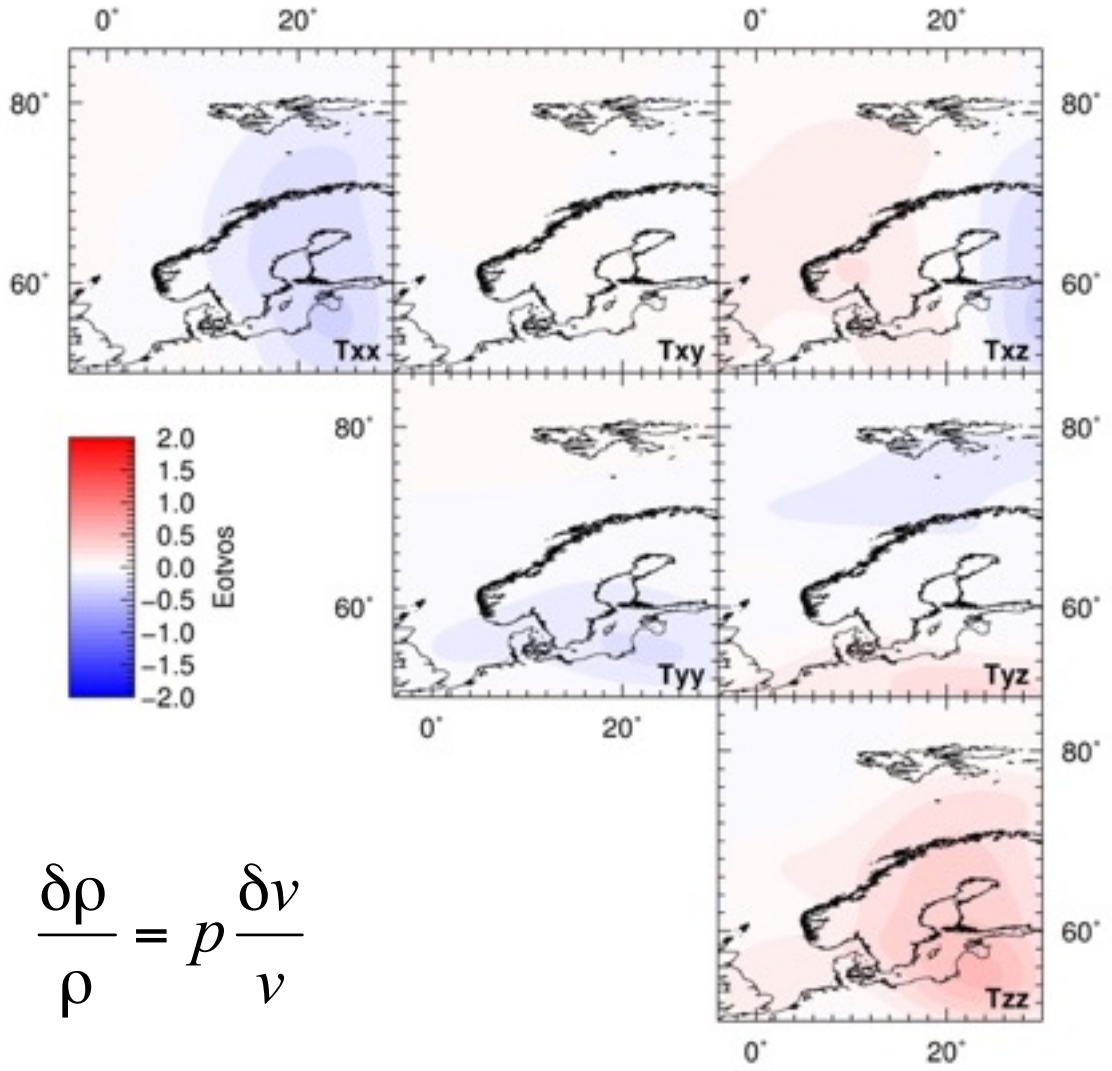

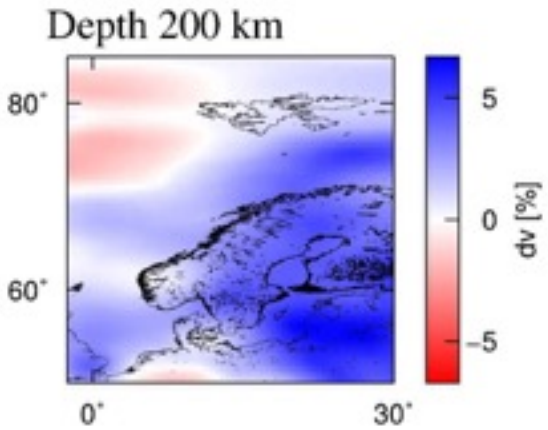

$$\frac{\delta\rho}{\rho} = p\frac{\delta v}{v}$$

Global tomographic models

Christian-Albrechts-Universität zu Kiel

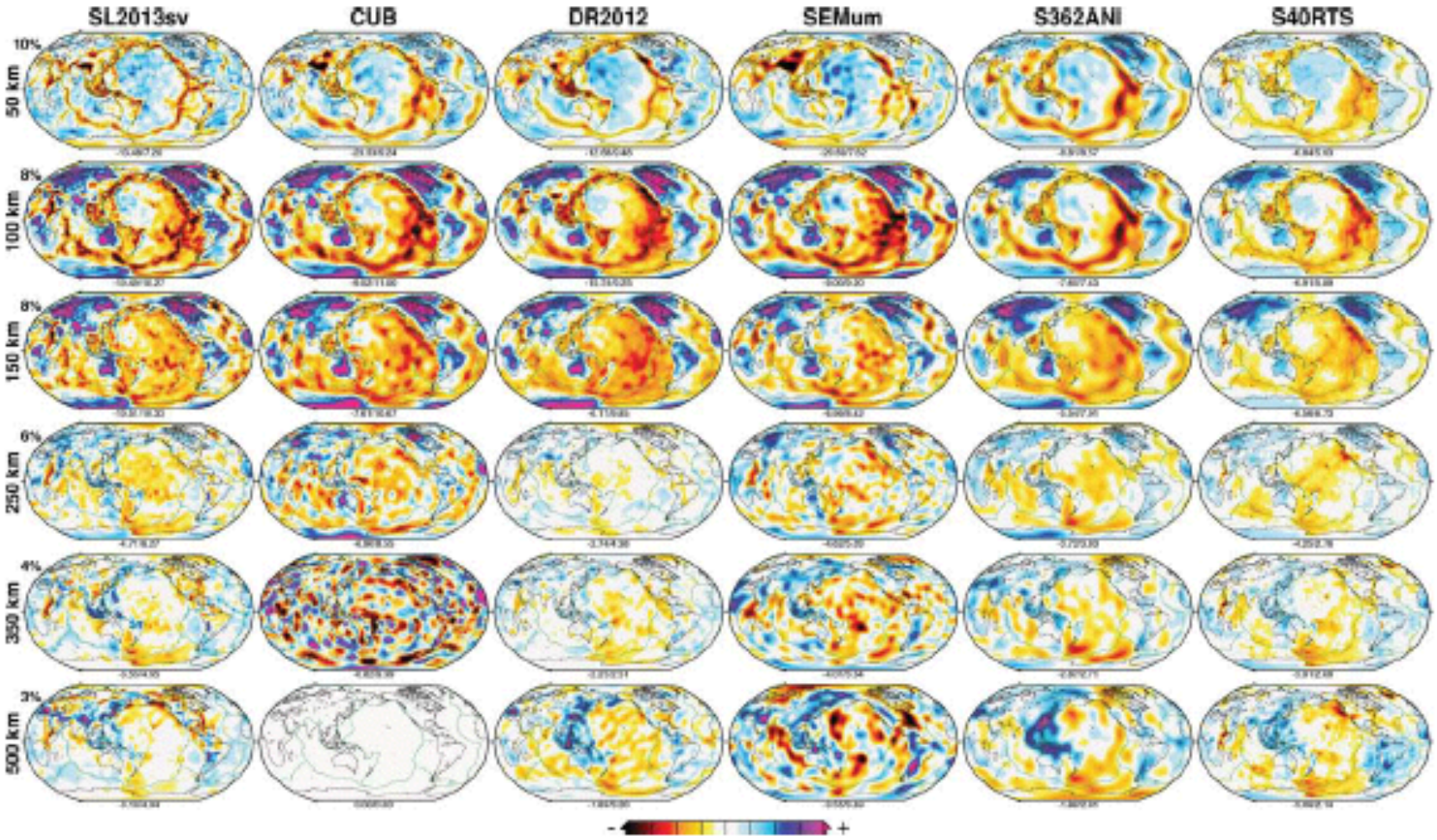

Schaeffer & Lebedev 2013

Recommended reading

Afonso, J. C., M. Fernàndez, G. Ranalli, W. L. Griffin, and J. A. D. Connolly (2008), Integrated geophysical-petrological modeling of the lithosphere and sublithospheric upper mantle: Methodology and applications, *Geochem. Geophys. Geosyst.*, *9*(5), 10.1029/2007GC001834.

Artemieva, I., 2009. The continental lithosphere: Reconciling thermal, seismic, and petrologic data. Lithos, 109, 23-46.

Artemieva, I., 2011: The lithosphere – an interdisciplinary approach. Cambridge University Press.

http://www.lithosphere.info/research.html

Connolly, J. (2005), Computation of phase equilibria by linear programming: A tool for geodynamic modeling and its application to subduction zone decarbonation, *Earth and Planetary Science Letters*, *236*(1-2), 524–541, 10.1016/j.epsl.2005.04.033.

Eaton et al. 2009. The elusive lithosphere–asthenosphere boundary (LAB) beneath cratons. Lithos, 109, 1-22.

Fullea, J., J. C. Afonso, J. A. D. Connolly, M. Fernàndez, D. García-Castellanos, and H. Zeyen (2009), LitMod3D: An interactive 3-D software to model the thermal, compositional, density, seismological, and rheological structure of the lithosphere and sublithospheric upper mantle, *Geochem. Geophys. Geosyst.*, *10*(8), 10.1029/2009GC002391.